7-1-2016

CALIBRATION AND APPLICATION OF A SILICA-WATER SINGLE MINERAL THERMOMETER TO GEOTHERMAL SYSTEMS IN ICELAND AND CHILE

Jordan Anne Gibbons

Jordan Anne Gibbons

Candidate

Earth and Planetary Sciences

Department

This thesis is approved, and it is acceptable in quality and form for publication:

Approved by the Thesis Committee:

Dr. Zachary Sharp, Co-Chairperson

Dr. Peter Fawcett, Co-Chairperson

Dr. Laura Crossey

CALIBRATION AND APPLICATION OF A SILICA-WATER SINGLE MINERAL THERMOMETER TO GEOTHERMAL SYSTEMS IN ICELAND AND CHILE

by

JORDAN ANNE GIBBONS

B.S, ENVIRONMENTAL SCIENCE, WESTFIELD STATE UNIVERSITY, 2010

THESIS

Submitted in Partial Fulfillment of the
Requirements for the Degree of

Master of Science
Earth and Planetary Sciences

The University of New Mexico
Albuquerque, New Mexico

July, 2016

ACKNOWLEDGEMENTS:

Thank you to my committee members for all of their assistance with this study (Drs. Zachary Sharp, Peter Fawcett, and Laura Crossey). I would like thank those in the Center for Stable Isotopes for teaching me everything I currently know about mass spectrometers and always being willing to help and show how to fix technical problems when the mass spec was not working (Drs. Karen Zeigler, Nicu-Viorel Atudorei, and Laura Burkemper). I would also like to thank Dr. Daniela van den Heuvel and Dr. Lianne Benning at the University of Leeds for contributing the samples from the geothermal power plant. Thank you to Dr. Martin Reich of CEGA at the Universidad de Chile for hosting me during my fieldwork at Puchuldiza and especially his student, Camilo Sánchez-Yañez, for taking the time help with everything throughout the entire trip. Thank you to my colleagues and friends for their invaluable feedback on presentations (Oleg Maltsev, Jeff Williams, Lauren Wheeler. Thank you to Neal Wostbrock for all the dinners while I write this thesis and, of course, to my dog, Buddha, for keeping me company on the late nights working.

CALIBRATION AND APPLICATION OF A SILICA-WATER SINGLE MINERAL THERMOMETER TO GEOTHERMAL SYSTEMS IN ICELAND AND CHILE

by

Jordan Anne Gibbons

B.S, Environmental Science, Westfield State University, 2010
M.S, Earth and Planetary Sciences, University of New Mexico, 2016

ABSTRACT

Triple oxygen isotope values of silica samples and formation water with tight temperature constraints from the Hellisheiði power plant in southwest Iceland and the natural Puchuldiza siliceous hot springs in northern Chile were used to evaluate potential fractionation effects of biogenic vs. abiogenic samples and silica samples of different crystallinity. Temperature estimates from the Hellisheiði power plant based on silica-water oxygen isotope thermometry are in excellent agreement with samples with measured temperatures, and lower for samples from within the heat exchanger where temperatures can only be estimated. The calculated θ values from this study are in close agreement with the calculated θ values from other studies and indicate a 0.00001 change in θ per degree Celsius at ~100°C.

In a real-time silica precipitation experiment at the hot springs in Puchuldiza of northern Chile, silica only precipitated at the air-water interface. Amorphous silica and coexisting waters were collected in active hot springs ranging in temperatures from 63-84°C. In all cases, the calculated temperatures were less than the measured temperatures, ranging from 38-48°C. Recrystallized paleosinter record higher temperatures, 69.5°C and 89°C. All samples appear to be in equilibrium in the triple oxygen isotope system. We

interpret all samples as recording the temperatures of their formation. The poorly crystalline modern samples likely precipitated at the air-water interface while the water was cooling, reaching saturation with respect to silica and preserving temperatures that are less than the measured geothermal water temperatures. In contrast, the more crystalline paleosinter samples record the temperature of hydrothermal recrystallization below the air-water interface. Silica re-precipitating from dissolved paleosinter in the presence of acidic fumarolic steam was not in equilibrium with the condensed steam water on the basis of the $\Delta'^{17}O$ values, which was not indicated by the $\delta^{18}O$ values alone. Triple oxygen isotope measurements are robust and can be used to estimate the temperature of formation, the isotopic composition of the formation water, and discern between equilibrium and non-equilibrium processes. Silica of different crystallinities and that were formed by abiogenic and biogenic processes all plot on the same silica-water fractionation line from the literature.

TABLE OF CONTENTS

LIST OF FIGURES viii

LIST OF TABLES iv

INTRODUCTION 1

Geothermal Systems 1

Triple Oxygen Isotope System 3

METHODS 7

Field Sampling: Iceland 7

Field Sampling: Chile 9

Scanning Electron Microscope (SEM) and X-ray Diffraction (XRD) Analysis 13

Isotope Analysis 13

RESULTS 16

Iceland Results 16

Chile Results 20

DISCUSSION 28

Iceland 28

Chile 31

CONCLUSION 34

APPENDICES **36**

APPENDIX I: Description of samples 37

APPENDIX II: Raw data from the Hellisheiði power plant 39

APPENDIX III: Raw data from the Puchuldiza geothermal field 40

APPENDIX IV: Basalt-water mixing model 41

APPENDIX V: Evaporation model 42

REFERENCES **43**

LIST OF FIGURES

FIGURE 1: Map of the Hellisheiði power plant location....**8**

FIGURE 2: Schematic the Hellisheiði power plant....**8**

FIGURE 3: Backscattered electron image of silica sample R9 (60ºC) from the Hellisheiði power plant....**9**

FIGURE 4: Map of Puchulidza geothermal field location....**10**

FIGURE 5: Aerial imagery the Puchulidza gothermal field....**11**

FIGURE 6: Overview of the study site in Puchuldiza....**12**

FIGURE 7: SEM and XRD images of samples from the Hellisheiði power plant....**15**

FIGURE 8: Graph of the δD-$\delta^{18}O$ values of water from the Hellisheiði power plant and the Puchuldiza hot spring area....**16**

FIGURE 9: Graph of the calculated temperatures based on oxygen isotopic values....**17**

FIGURE 10: Graph of the Hellisheiði samples and water in $\Delta'^{17}O$-$\delta'^{18}O$ space....**18**

FIGURE 11: Graph of θ vs Temperature from the Hellisheiði samples....**19**

FIGURE 12: SEM images and corresponding XRD analyses of samples from the Puchuldiza geothermal field....**21**

FIGURE 13: Graph of the Puchuldiza samples and water in $\Delta'^{17}O$-$\delta'^{18}O$ space....**23**

FIGURE 14: Example of glass microscope slide used in the real-time silica-precipitation study....**24**

FIGURE 15: Graph depicting θ vs temperature from the Puchuldiza samples....**27**

FIGURE 16: Graph of silica saturation line in relation to the silica concentration from of the hot springs in the Puchuldiza geothermal field....**30**

FIGURE 17: Graph of $1000\ln\alpha^{18}_{qz\text{-}wt}$ vs. measured temperature ($10^6/T^2$)....**32**

LIST OF TABLES

TABLE 1: pH and temperature measurements from Puchuldiza hot spring **22**

INTRODUCTION

Geothermal Systems:

The presence of siliceous springs indicate extensive water-rock interaction with a geothermal system that is greater than 175°C at depth (Fournier and Rowe, 1966). As the geothermal spring water cools and reaches the surface, deposition of siliceous sinter occurs (hereafter referred to as "sinter"). Factors governing silica precipitation are evaporation and temperature decrease (e.g. Jones et al., 2000; Guidry and Chafetz, 2002; Mountain et al., 2003; Tobler et al., 2008; Nicolau et al., 2014), where evaporative water loss and/or cooling results in supersaturation of water with respect to amorphous silica. Sinter deposits can be composed of multiple silica phases including amorphous silica, Opal C/CT, and quartz (Herdianita et al., 2000; Campbell et al., 2001; Lynne and Campbell., 2003; Lynne and Campbell, 2004; Rodgers et al., 2004; Lynne et al., 2005, 2006, 2007, 2008; García-Valles et al., 2008; Nicolau et al., 2014). Initial deposition is always as amorphous silica while diagenesis to more stable phases is suggested to occur post-deposition, kinetically with high temperature fluid, and/or fumarolic activity (Lynne and Campbell, 2004). Sinter normally forms in near-neutral pH waters, with a high silica content, and variable anion and cation concentrations (Nicolau, 2013 and studies therein) or as a residue of re-precipitated silica present in an acidic fumarole (White et al., 1956, Rodgers et al., 2004). Macroscopic silica structures are formed with different textures informally called lily pads, mounds (geyserite), rimming, terraces, and discharge aprons that are loosely related to temperature (Cady and Farmer, 1996; Lynne, 2012). Many of these textures are maintained even when the spring is no longer active and they can survive diagenesis (Lynne, 2012; Lynne and Campbell, 2004), making fossil sinter

deposits (hereafter referred to as “paleosinter”) an excellent resource for tracking hydrological conditions of the geothermal system.

Geothermal power plants can be used to study sinter formation in a more controlled setting than what is found in the unconstrained conditions of a hot spring (ie, Kita et al., 1985; Inagaki et al., 2003; Aramaki et al., 2005; Yanagisawa et al., 2008; Meier et al., 2014; Pambudi et al., 2015). Silica precipitates as amorphous silica in the plant’s pipes and is known as “scaling”. Numerous studies have been made to better understand sinter formation, with the ultimate goal of reducing silica precipitation because the scaling can cause pipe blockages (ie, Fleming and Crerar, 1982; Harrar et al., 1982; Henley, 1983; Gallup, 2002; Gunnarsson and Arnorsson, 2002; Gallup and Barcelon, 2005; Amjad and Zuhl, 2008; Sigfusson and Gunnarsson, 2011; Stapleton and Weres, 2011).

Both siliceous springs and geothermal power plants offer a unique site for the study of silica-water precipitation in terms of oxygen isotope fractionation. Geothermal power plants provide almost a laboratory-type experiment where the water flow and temperature are nearly constant, reducing the number of unconstrained variables when looking at silica-water fractionation. Siliceous hot springs are natural systems that can be used to test the conditions at which silica actually precipitates and how the oxygen isotopic composition might be modified over time. Many studies have looked at the oxygen-18 ($\delta^{18}O$) ratio of geothermal water (*e.g.*, Arnòrsson, 1975; Giggenbach, 1978; Guidry and Chafetz, 2002; Geilert et al., 2015; Pope et al., 2010, 2016) or silica formed in geothermal water (e.g., Murata et al., 1977; Hayashi, 2013), but only two studies, to our knowledge, have measured both the water and the silica in either a geothermal power

plant (Kita et al., 1985) or siliceous hot springs (Sharp et al., 2016). These systems have the potential to provide excellent temperature control to calculate silica-water fractionation over a temperature range that is difficult to duplicate in the laboratory (34-250°C).

A recent calibration of the triple oxygen isotope system used a sinter sample and coexisting formation water in a siliceous hot spring from Yellowstone National Park, U.S.A, a marine chert sample, and silica from marine diatom frustules (Sharp et al., 2016). The marine diatoms are of biogenic origin, leaving the importance of any 'vital effect' ambiguous. All samples used in the Sharp et al. (2016) single mineral thermometer were amorphous silica and it is unknown if the silica-water fractionation depends on crystallinity. Silica samples and the formation water with tight temperature constraints from geothermal power plants and siliceous hot springs with multiple silica polymorphs allow us to test the robustness of the new single mineral thermometer in terms of biogenic vs. abiogenic samples and samples of different silica crystallinity.

Triple Oxygen Isotope System

Terrestrial minerals generally plot on a straight line with a slope (λ) of ~0.525 in $\delta^{17}O$-$\delta^{18}O$ space where:

$$\delta\,{}^{x}O = \left(\frac{\left(\frac{{}^{x}O_{sample}}{{}^{16}O_{sample}} \right)}{\left(\frac{{}^{x}O_{standard}}{{}^{16}O_{standard}} \right)} - 1 \right) \times 1000 \qquad 1).$$

x is either mass 17 or 18. The empirical fit was termed the Terrestrial Fractionation Line (TFL) and has a near perfect relationship with an R^2 value of 0.999 (Clayton, 2003; Rumble et al., 2007). Therefore, to a first approximation, the information provided by

$\delta^{17}O$ values adds nothing to that obtained by $\delta^{18}O$ values alone. The equilibrium fractionation of $\delta^{17}O$ between any two phases a and b is defined as:

$$\alpha^{17}O_{a-b} = (\alpha^{18}O_{a-b})^{\theta} \quad 2)$$

where $\alpha_{a\text{-}b}=R_a/R_b$ and R is either $^{17}O/^{16}O$ or $^{18}O/^{16}O$ and θ ranges from 0.5 to 0.5305 for equilibrium or kinetic reactions (Cao and Liu, 2011). Deviations from the TFL can be tens of per mil in extraterrestrial samples (Clayton et al., 1973) or stratospheric samples resulting from photochemical reactions (Thiemens & Heidenreich, 1983). However, with improved analytical techniques, slight variations from the TFL in terrestrial samples can now be measured and have been found to have geological significance. Variations above or below the TFL are expressed as:

$$\Delta'^{17}O = \delta'^{17}O - \lambda \times \delta'^{18}O + \gamma \quad 3)$$

where λ is the reference slope and γ is the y-intercept. In this work, we use a λ value of 0.528 because this is the slope of the meteoric water line in triple oxygen isotope space and a γ value of 0.0. Because of the relationship expressed in equation 2, the TFL has a slight curve, which is removed when plotted in 'linearized notation' where $\delta' = 1000 \text{ X } \ln(\delta^{x}O/1000 +1)$, where x is either mass 17 or 18. This allow us to directly compare variations over the full range of $\delta^{18}O$ values along the TFL (Miller, 2002). By combining and rewriting the equilibrium fractionation equation with δ′ notation, the mass-dependent equilibrium fractionation between two phases can be written as $1000\ln\alpha_{a\text{-}b} = \delta'^{x}O_a - \delta'^{x}O_b$.(where x is either mass 17 or 18).

While λ is used to describe the slope of the best fit, we use θ to describe calculated equilibrium processes that are thermodynamically dependent and is defined for the triple oxygen isotope system as:

$$\theta_{a-b} = \frac{\delta'^{17}O_a - \delta'^{17}O_b}{\delta'^{18}O_a - \delta'^{18}O_b} \quad 4)$$

where *a* and *b* are any mineral pair but for this study we will use silica and water. A temperature dependence on the θ of equilibrium processes was proposed theoretically (Urey, 1947; Matsuhisa et al., 1978; Young et al., 2002; Cao and Liu, 2011) and derived empirically for the silica-water mineral pair (Pack and Herwartz, 2014; Sharp et al., 2016). Cao and Liu (2011) calculated a range of θ values with 0.5305 at infinite temperature (for all equilibrium oxygen isotope fractionation) and 0.5242 at 0°C (for silica-water oxygen isotope fractionation). Sharp et al. (2016) empirically found a slightly lower $\theta_{\text{silica-water}}$ (0.5235-0.5240) at 0°C when analyzing the silica from marine diatoms.

The many experimental studies characterizing the temperature dependence on silica-water fractionation using $\delta^{18}O$ values were compiled in Sharp et al. (2016). They determined a best-fit of all previous experimental studies, given by the following equation:

$$1000 ln\alpha^{18}_{a-b} = \frac{4.28\ (\pm 0.07) * 10^6}{T^2} - \frac{3500\ (\pm 200)}{T} \quad 5)$$

where T is in Kelvin. Using a variety of biogenic and abiogenic silica samples over a temperature range of 0°C-47°C, Sharp et al. (2016) also calculated the temperature $\delta'^{17}O$ relationship:

$$1000 ln\alpha^{17}_{a-b} = \left(\frac{4.28\ (\pm 0.07) * 10^6}{T^2} - \frac{3500\ (\pm 200)}{T}\right) * \left(0.5305 - \frac{1.85\ (\pm 0.04)}{T}\right) \quad 6)$$

Combining the two equations and solving for $\Delta'^{17}O$, provides a potential single mineral thermometer where:

$$\Delta'^{17}O_a - \Delta'^{17}O_b = \left(\frac{4.28\ (\pm 0.07) * 10^6}{T^2} - \frac{3500\ (\pm 200)}{T}\right) * \left(0.5305 - \frac{1.85\ (\pm 0.04)}{T} - \lambda_{RL}\right) \quad 7)$$

where λ_{RL} is arbitrary but is taken as 0.528 in this study, in order to parallel the meteoric water line (Sharp et al., 2016).

Here, we apply the silica-water triple oxygen isotope thermometer to silica and the formation water from the Puchuldiza hot springs in northern Chile and the Hellisheiði power plant in Iceland to a higher temperature range of 60-118°C. The triple oxygen isotope silica-water fractionation provides a rigorous test as to whether the silica in these geothermal systems formed in equilibrium with the formation water and the temperature of formation. This study will explore whether biogenic silica precipitates in isotopic equilibrium with the formation water or shows a vital effect and if different silica polymorphs have different silica-water fractionations.

METHODS

Field Sampling: Iceland

Sinter and water samples from the Hellisheiði geothermal plant were provided by Daniela van den Heuvel and Liane Benning (University of Leeds, England). Samples were from silica scaling in a heat exchanger located at the Hellisheiði power plant, about 25 km southeast of the capital city of Reykjavik in southwest Iceland (Fig. 1). The Hellisheiði power plant is located in a graben of the Hengill central volcano along a NE-SW trending fault (Franzson et al., 2005). The plant covers 8 km^2 and contains 3 separation stations connected to 30 production wells (Hallgrímsdóttir et al., 2012). The hydrothermal plant uses a 250-300°C aquifer located at 2 km depth fed by meteoric water (Meier et al., 2014). The power plant brings the water up from depth, releases pressure, dropping the temperature to ~120ºC and uses the steam produced to generate electricity. The remaining water after steam separation is slightly basic with low salinity and supersaturated with respect to silica. The dissolved silica content ranges from 758-795 ppm, about 200-300 ppm higher than amorphous silica saturation at 120ºC (Fournier and Rowe, 1966). The remaining water is pushed through two heat exchangers bringing the water from 120°C to 60°C. The water is then combined back with the steam condensate and injected back into the subsurface (Fig. 2).

Steam separation results in liquid that is supersaturated with respect to silica. The water tends to precipitate the silica as colloidal silica under turbulent conditions (such as a heat exchanger) that aggregate on the insides of pipes and machinery (Fig. 3) and cause clogging if not properly cleaned on a regular basis (about 6-8 months). The silica for this study was extracted from the heat exchanger in January

Figure 1: Map of where the Hellisheiði power plant is located. Imagery from ESRI online.

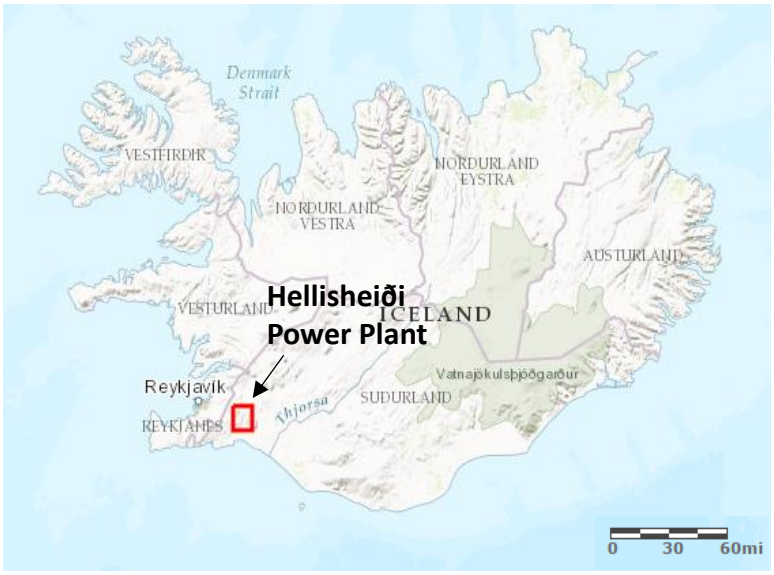

2014 during one of the cleaning processes. Six silica samples were collected: one from the inlet (118°C ±0.5), one from the outlet (60°C ±2.0), and four from chambers inside the heat exchanger with estimated temperatures of 100°C, 85°C, 75°C, and 70°C. Variability of the temperatures inside the heat exchanger is unknown. Silica samples were dried at 40°C and stored in plastic containers. Water could only be sampled at the inlet (118°C) and outlet (60°C) of the heat exchanger. Water samples were stored in airtight containers and kept in a refrigerator to minimize evaporation.

Figure 2: Schematic of the heat exchanger of the Hellisheiði power plant in Iceland.

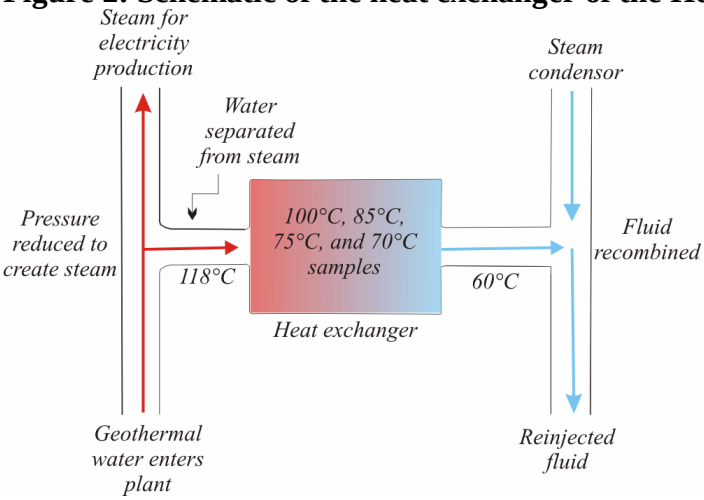

Figure 3: Backscattered electron image of silica sample R9 (60ºC) from the Hellisheiði power plant in Iceland. The small spheres aggregate on the insides of pipes to form a larger, bulbous texture and can clog pipes and machinery.

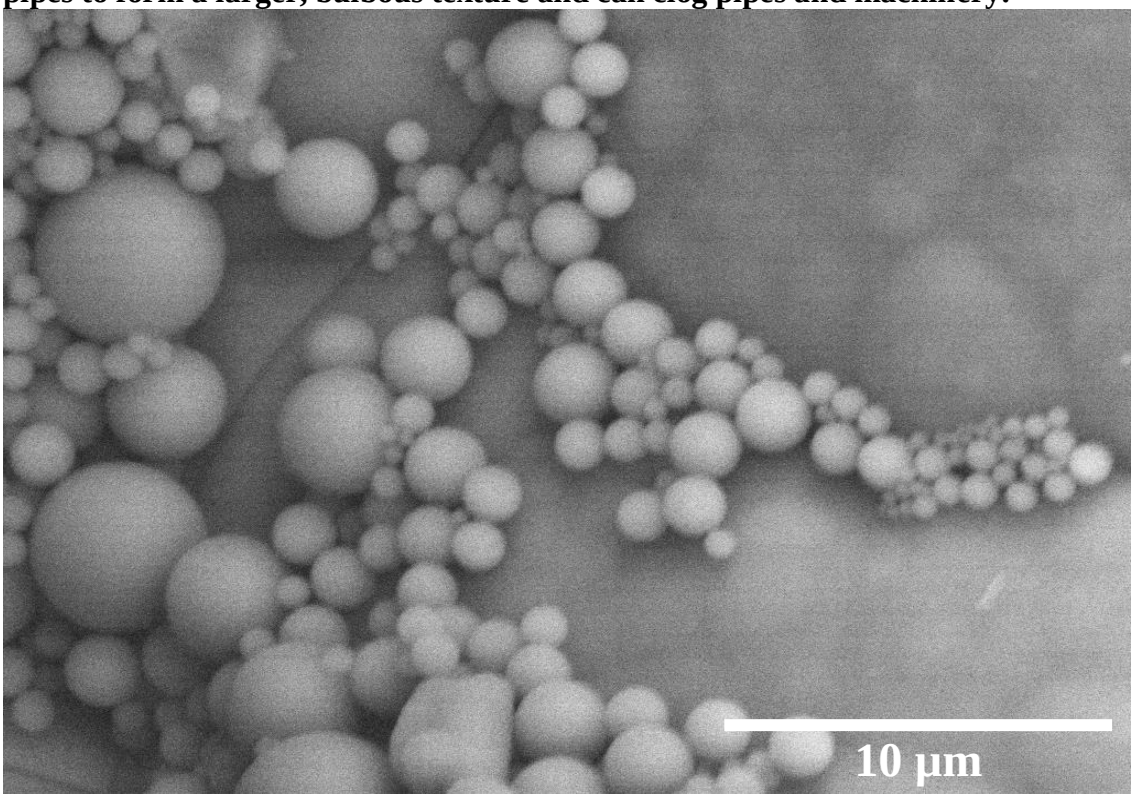

Field sampling: Chile

The Puchuldiza hot springs are located in the Tarapacá Region of the Andean Cordillera, 160 km northwest of Iquique in northern Chile (S 19° 24' 24.2", W 068° 57' 25.8", Fig. 4). The geothermal field is about 1 km^2 and located at an elevation of 4200 meters above sea level (m.a.s.l, Fig. 5). The geothermal field is located in a small graben on top of Quaternary volcanic rock ranging from basalt to rhyolite in the middle of N-S, NW-SE, and NE-SW fault systems (Lahsen et al., 2005). The oldest geologic unit is Cretaceous in age and consist of shales, sandstones, and conglomerates (Lahsen et al., 2005). Temperatures of water at depth are thought to be between 180-210°C based on Na/K ratios and silica water content modeled with adiabatic expansion of hot water

Figure 4: Map of northern Chile showing the Puchulidza geothermal field in relation to cities of that region (adapted from Sánchez-Yañez et al., 2016).

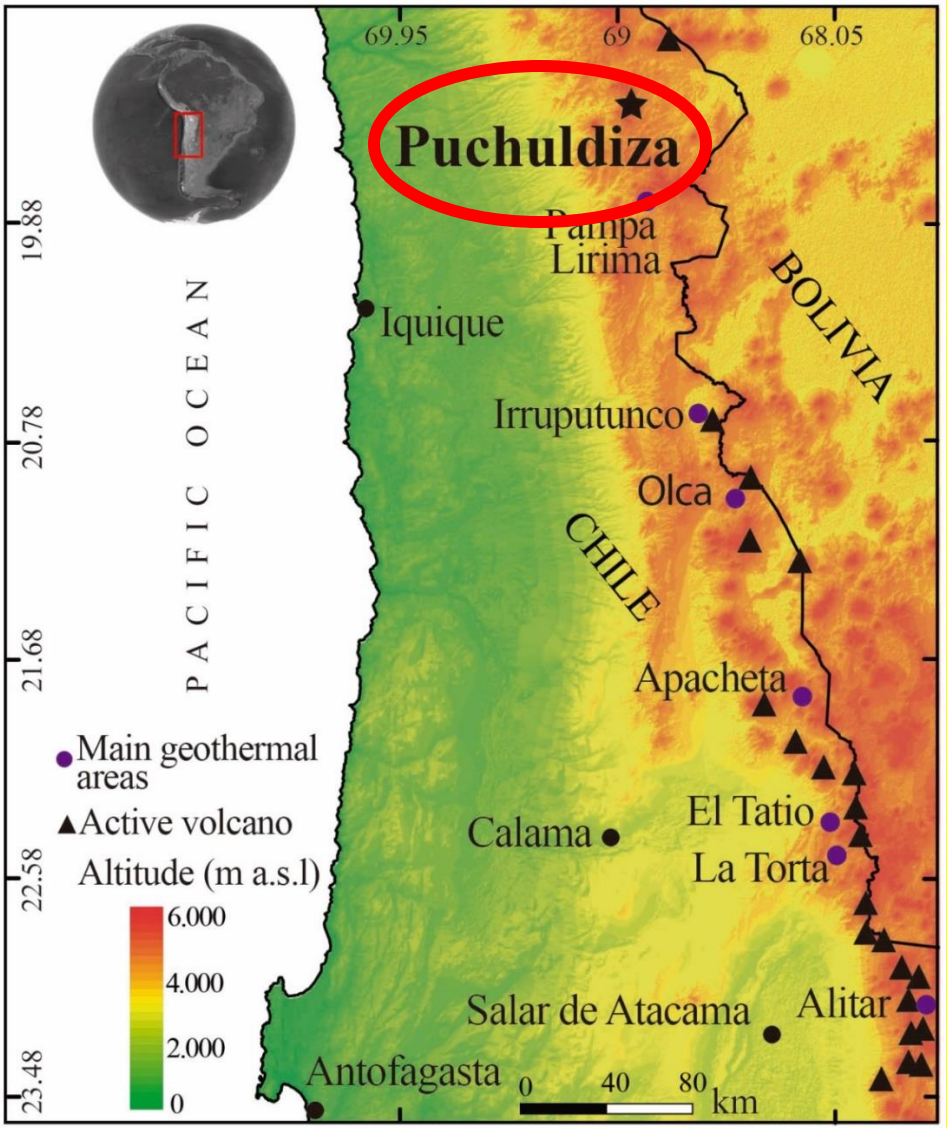

coming to the surface (Mahon and Cusicanqui, 1980; Lahsen et al., 2005; Tassi et al., 2010). The hot springs generally have temperatures near boiling (86.4ºC at 4200 m.a.s.l), although there are a few springs that have lower temperatures. Water chemistry of the surface expressions are slightly basic in pH (7.4-8.4), alkali-chloride type, with a silica content ranging from 110-186 ppm, under saturated with respect to amorphous silica at 85ºC (Fournier and Rowe, 1966). Sinter and water samples were collected in March 2016

in collaboration with Camillo Emmanuel Sánchez Yáñez and Martin Reich, Centro de Excelencia en Geotermia de Los Andes (CEGA) at the University of Chile, Santiago.

Both silica and water were collected at various sites from the spring source, downstream to lower temperatures (Fig. 6). In order to collect freshly precipitated silica, glass microscope slides were placed at 3 temperature locations (85°C, 70°C, and 63°C; Fig. 6). Two glass slides were placed with some of the slide exposed to air and two slides were completely submerged. Sinter was sampled near the area where the glass slides were placed and stored for future analysis. Water was sampled at the time the plates were installed and after the plates were removed. Water was stored in 25ml plastic

Figure 5: Aerial imagery of the 1 km^2 region of the Puchulidza gothermal field with locations of springs numbered. The spring from this study is number 12, marked with a red star (adapted from Sánchez-Yañez et al., 2016).

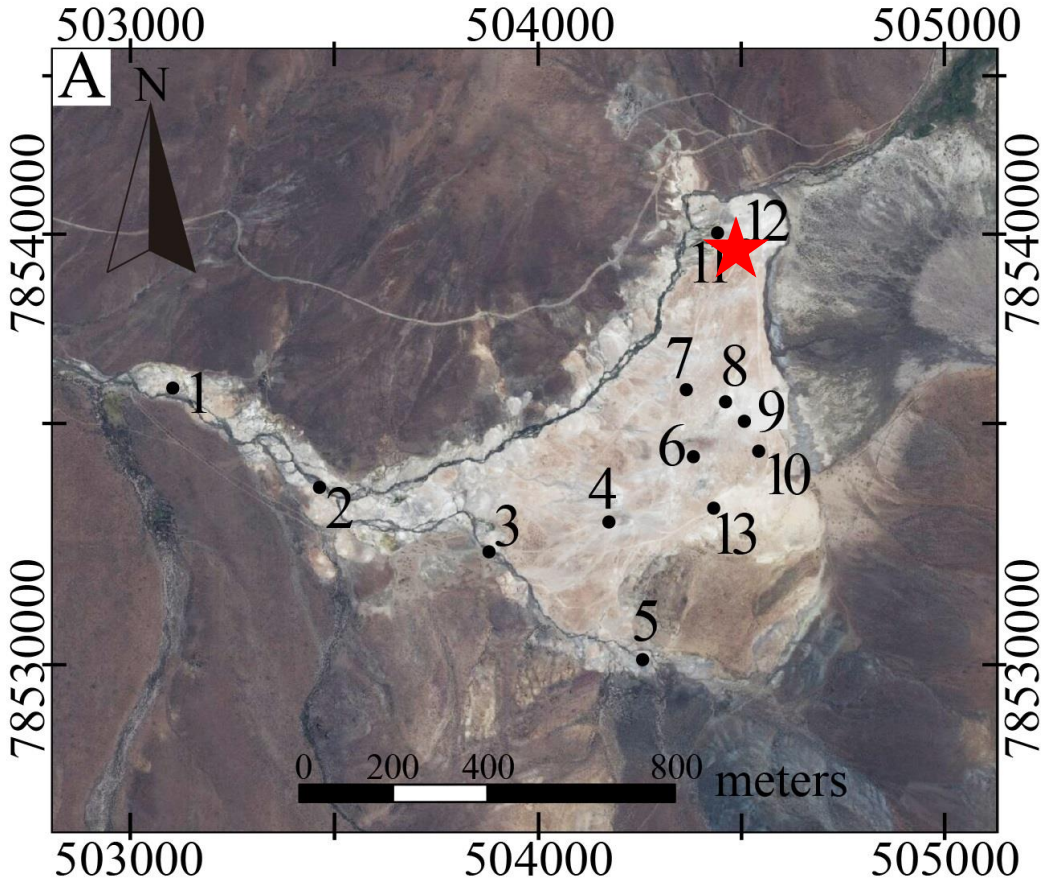

bottles and refrigerated upon arrival at the University of New Mexico. Glass microscope slides were installed for 9 days and then wrapped in aluminum foil until they could be weighed and dried at the University of New Mexico. Temperature and pH were measured at each glass slide location in the afternoon on installation day, mid-morning on day 4, before sunrise on day 5 and in the afternoon on the removal day in order to track variations in temperature of the spring during the silica precipitation period. A sample of silica precipitate that occurred in a fumarole was also collected as well as condensed steam. Sinter that has undergone diagenesis below the water's surface from springs that no longer contained water were also sampled and labelled "paleosinter".

Figure 6: Overview of the hot spring in Puchuldiza. Rock stacks are places were glass slides were located. Bubbling spring is 84.6°C, which is boiling at the elevation of the springs.

Scanning Electron Microscope (SEM) and X-ray Diffraction (XRD) Analysis:

Silica samples were imaged and analyzed qualitatively using a JEOL 82000 SEM. Analytical conditions were an accelerating voltage of 15 kV, stage height of 14 mm, spot size of 8, and an aperture location of 1. Crystallinity was determined from powder X-ray diffraction. About 200 mg of each silica sample was analyzed using a Rigaku D/teX X-ray diffractometer. Copper Kα radiation was used as an X-ray source and the sample's X-ray spectra was obtained using a scan rate of 6.2 deg/min with a 0.02 deg step. Jade whole pattern fitting software was used for data analysis.

Isotope Analysis

Silica samples were treated in 6M HCl to remove carbonate. Visible bubbling stopped after several hours. The samples were then rinsed with distilled water and dried at 60°C. The oxygen isotope composition of the purified silica was measured using laser fluorination (Sharp, 1990). Silica samples were loaded onto a nickel sample plate with 1-2 mg of sample per hole. Samples were pre-fluorinated to remove any hydroxyl oxygen (Dodd and Sharp, 2010). The samples were allowed to react with BrF_5 at room temperature until the hydroxyl oxygen was removed, usually 30-60 min. Laser heating was performed with a CO_2 laser and BrF_5 as a fluorinating agent (Sharp et al., 2016). The evolved oxygen (O_2) was separated from the excess BrF_5 and other contaminating gases (*e.g.*, SiF_4) using a series of liquid nitrogen cold traps. The oxygen was passed through a warm salt (NaCl) trap to remove any trace amounts of F_2 gas that may have been produced. The oxygen was trapped using a 5Å molecular sieve. The molecular sieve was heated to release the oxygen in a stream of helium carrier gas that carried the oxygen

through a 5Å mol sieve GC column. The GC column separated the oxygen from any trace NF_3 contamination to minimize interference of oxygen-17 by NF_3.

Water was fluorinated for O_2 analysis by reacting a 1-2 µL aliquot of water with BrF_5 in a ¼ inch nickel tube for 4 minutes at ~150°C as described in O'Neil and Epstein (1966). The oxygen released during the reaction was purified in the same manner as the oxygen from silica.

The purified O_2 from each sample is analyzed with respect to the Center for Stable Isotope's (CSI) laboratory O_2 standard which has been calibrated to VSMOW, SLAP, NBS-28 and San Carlos Olivine. Oxygen isotope analyses were made using a Finnigan MAT 253 mass spectrometer. Each analysis consisted of a minimum of 30 iterations of 24 second integration time for both the sample and the standard. Long counting times of about 1-1.5 hours are necessary to achieve $\Delta'^{17}O$ values with precision of ±0.005‰ (Luz and Barkan, 2010; Pack and Herwartz, 2014). All values are reported in per mil (‰) notation. The standard deviation (1σ) are for $\delta^{17}O$ values is 0.05‰ and 0.1‰ for $\delta^{18}O$ values.

Figure 7: SEM and XRD images of samples from the Hellisheiði power plant. a) Sample of amorphous silica from the sample location corresponding to 118ºC (sample F.1) and corresponding XRD spectra. b) Sample of amorphous silica from sample location corresponding to 60ºC (sample R.9). The XRD analyses show clear amorphous silica peaks (XRD analyses and SEM images from UNM).

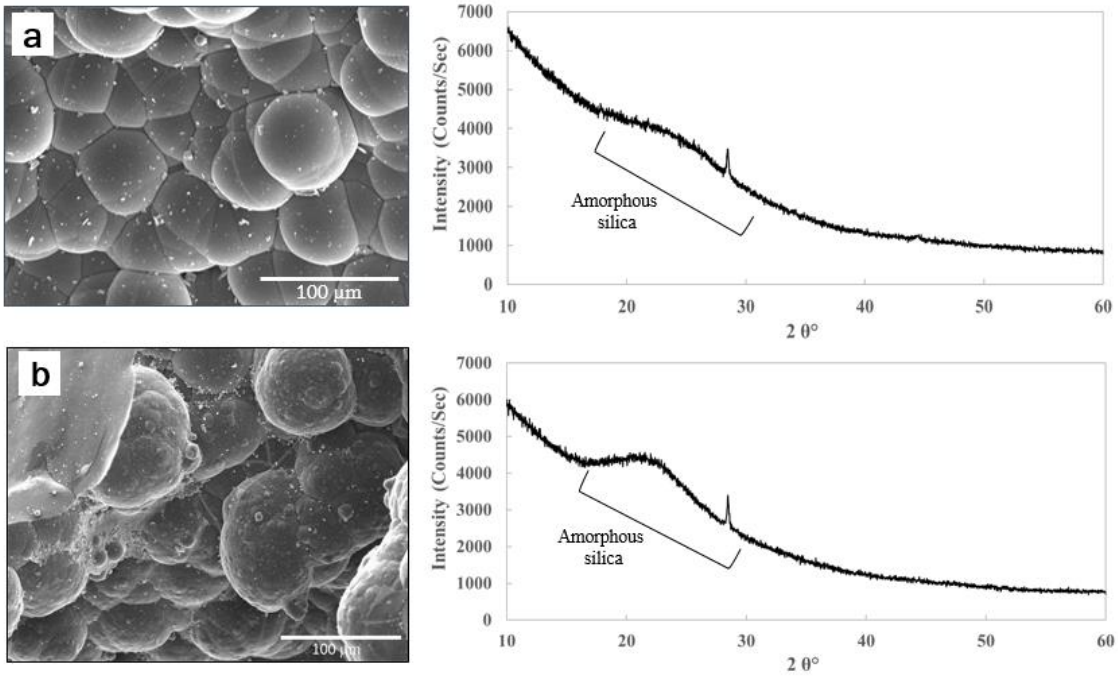

RESULTS

All data is reported in Tables 1 and Appendices I, II, and III.

Iceland Results:

SEM and XRD analyses indicated that all samples were amorphous silica (Fig. 7). A difference of 0.3‰ in $\delta'^{18}O$ and 0.001‰ in $\Delta'^{17}O$ was observed between the water samples at 118°C and 60°C. Since the isotopic value did not significantly change, silica samples collected at all temperatures were assumed to be in equilibrium with water of the same isotopic composition. The geothermal water has a $\delta^{18}O$ value that is 2‰ heavier than the $\delta^{18}O$ value of cold water wells and 5‰ lighter than the reported range of δD values (Mutonga, 2007; Fig. 8). These results imply that the water in the geothermal

Figure 8: Graph showing δD-$\delta^{18}O$ values of water from the Hellisheiði power plant and the Puchuldiza hot spring area. Blue circles show the cold water (Mutonga, 2007) plot on the global meteoric water line (GMWL) while the hot water shows water-rock interaction (blue arrow). Green triangle is cold, stream water (Mahon and Cusicanqui, 1980) and plots near the GMWL while the hot spring water (green circle) shows some rock-water interaction. The yellow circle is the isotope value of the condensed steam from a Puchuldiza fumarole and plots on an evaporation trend (yellow arrow) from the geothermal water.

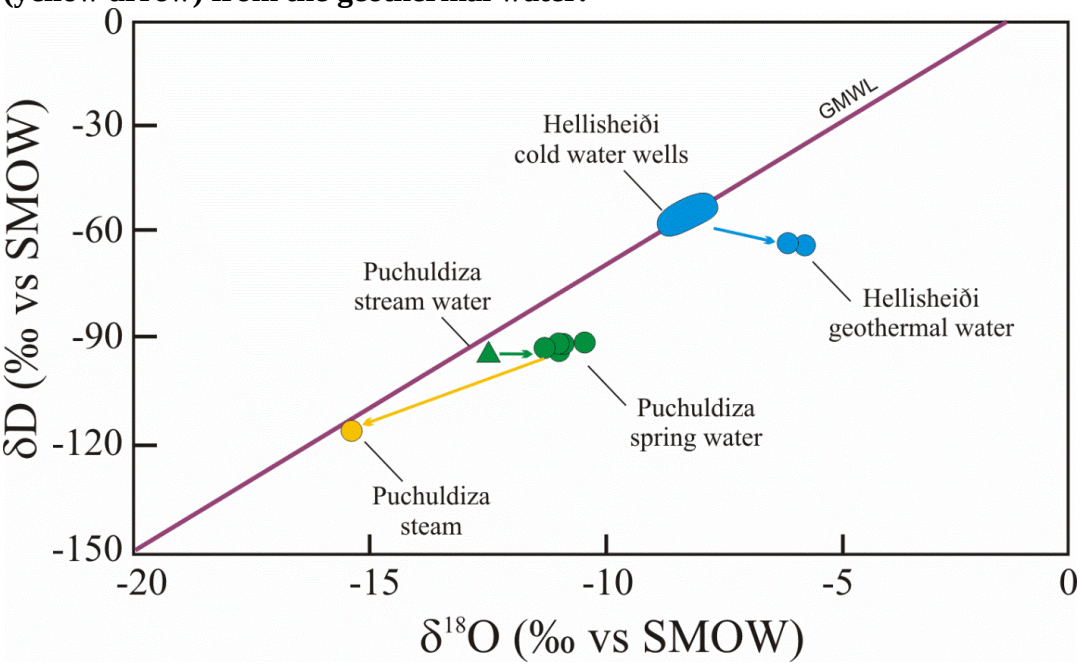

power plant underwent some evaporation to drive $\delta^{18}O$ and δD values lower (Craig and Gordon, 1965). After evaporation, the $\delta^{18}O$ values became heavier by water-rock interaction. The $\Delta'^{17}O$ values of the geothermal waters are lower than typical meteoric water, also consistent with evaporation (Luz and Barkan, 2010). The isotopic value of the silica that precipitated from the water changed significantly from the 118°C sample ($\delta'^{18}O$=13.48‰, $\Delta'^{17}O$=-0.061‰) to the 60°C sample ($\delta'^{18}O$=22.03‰, $\Delta'^{17}O$=-0.092‰).

Temperatures were estimated using equations 5 and 6 and compared to the measured temperatures (Appendix II). The estimated temperatures varied by less than 1°C between equations 5 and 6 and the error of the temperature estimate is ±1.8ºC. Temperature estimates were significantly lower than measured temperatures for all samples except the 60ºC sample (Appendix II). The 100°C and 85°C samples were

Figure 9: Graph showing the calculated temperature using equations 5 and 6 (blue circles) and equation 7 (red triangles). Uncertainty in the calculated temperatures are the error bars. The line shows where samples would plot if the calculated temperatures were exactly the same as measured temperatures.

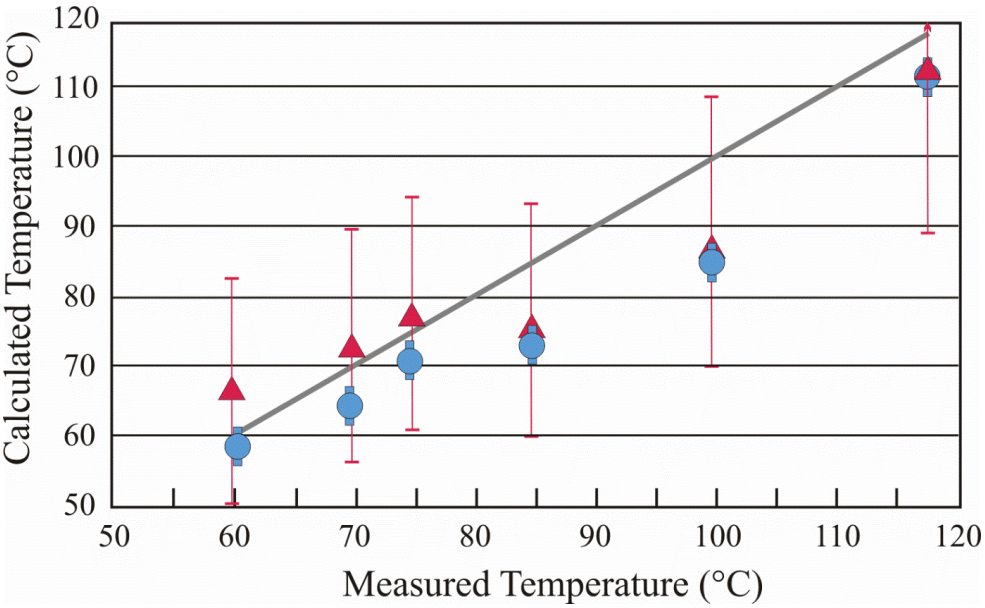

Figure 10: Graph of the Icelandic samples and water in $\Delta'^{17}O$-$\delta'^{18}O$ space with the single mineral thermometer fractionation line (Sharp et al., 2016). Samples plot on or very close to the fractionation line, indicate equilibrium processes. Diamonds are an individual analysis, error bars are the reported uncertainty and the lighter circles are to group the data in to samples.

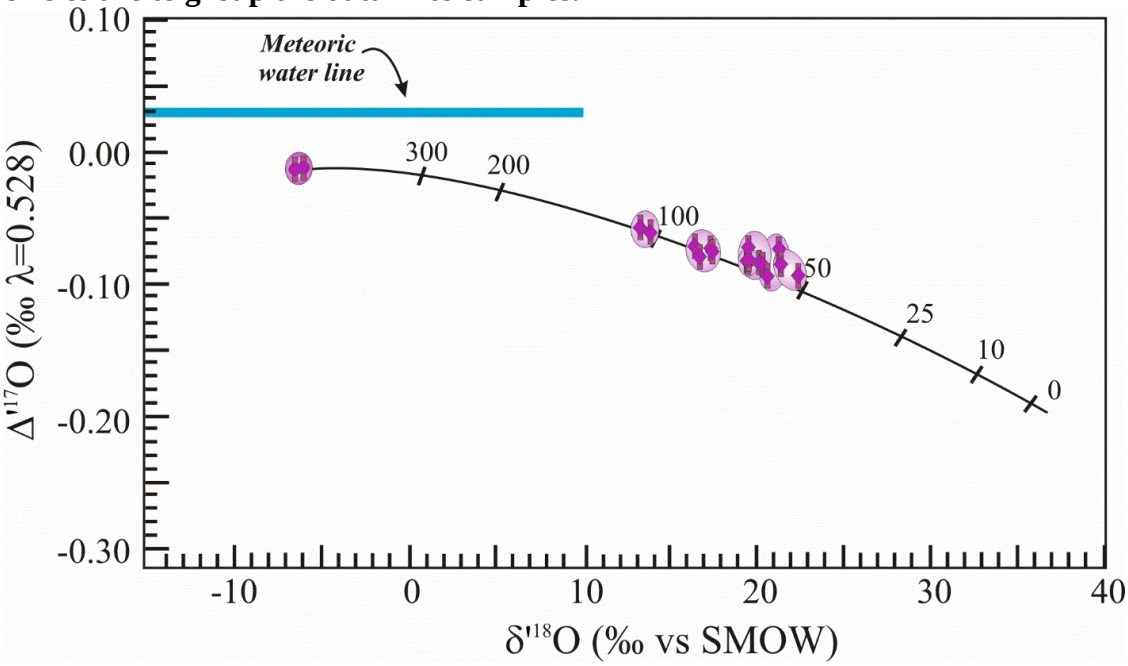

estimated to be 14ºC and 12°C too low, respectively. The temperature estimates for the 118°C and 70°C samples were about 6°C too low while the 75°C samples was 4.6°C too low. The 60°C sample was 0.1°C too low, identical to the measured temperature, within error. Using Eq. 7 to estimate temperatures produces more varied results because a slight shift in $\Delta'^{17}O$ values equates to a larger temperature shift than when using $\delta'^{18}O$ or $\delta'^{17}O$ values alone. Temperature estimates using equation 7 have an error of $^{+21}_{-17}$ °C. Equation 7 is less useful for temperature estimates but is beneficial to see if samples are in equilibrium because there is only one unique solution for equilibrium using triple oxygen isotope values. The higher temperature samples (118°C and 100°C) were 5°C and 12°C too low, respectively. The estimated temperature for the 85°C sample was 9°C too low. The 75°C and 70°C were estimated to be 2ºC above the measured temperature and 60°C

Figure 11: Graph depicting θ vs Temperature using Cao and Liu (2011) using dark grey triangles and Sharp et al. (2016) using light grey squares. The Iceland samples of this study in red when plotted using the measured temperature and green using the temperature calculated from equation 5. Samples plot where the best fit regression lines overlap.

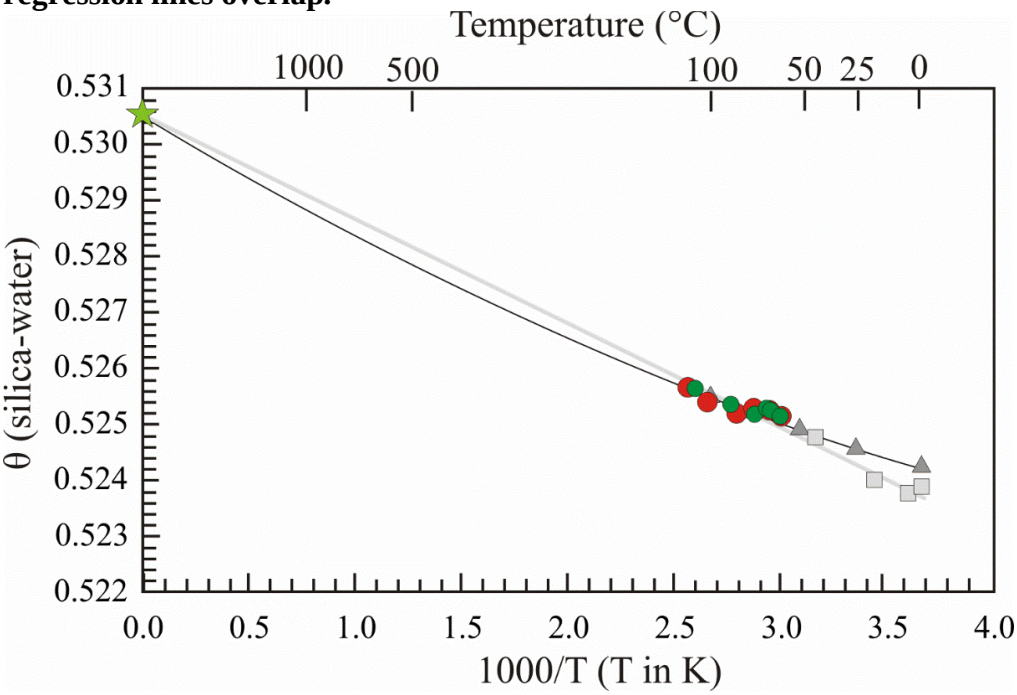

sample was estimated to be 7ºC above the measured temperature (Fig. 9). All the silica samples satisfy the conditions of equilibrium with the formation water in $\Delta'^{17}O$-$\delta'^{18}O$ space (Fig. 10).

The θ-T variation from 60-118ºC is 0.0005, corresponding to a 0.00001 change in θ per ºC over this temperature range. This is in excellent agreement with the θ-T relationship of Sharp et al. (2016) for quartz-water and Li et al. (2016) for carbonate-water. The calculated θ of the 118°C sample was 0.52572 while the 60°C sample was 0.52522 (Fig. 11). The best fit of the θ-T values of this study anchored at θ=0.5305 at T=∞ , where T is in Kelvin, is:

$$\theta = -\frac{(1.81 \pm 0.06)}{T} + 0.5305 \quad R^2 = 0.994 \qquad 8)$$

Equation 8 is within analytical error of the θ-T relationship of the samples from Sharp et al. (2016) and Cao and Liu (2011).

Chile Results:

SEM and XRD analysis showed that samples from the active hot spring were amorphous silica while the paleosinter is a more crystalline morphology (opal-CT and microcrystalline quartz, Fig 12). Surficial silica across the geothermal field is extremely friable. Recrystallized silica from below the surface, such as the eroded walls of springs no longer containing water (called paleosprings), are more lithified than the surficial silica. Some silica from the deepest part of the paleosprings, such as sample 7b, are hard, well-consolidated rock. The SEM images of sample 7b showed the well-consolidated samples are microcrystalline quartz (Fig. 12). The quantitative analysis of sample 7b showed a composition of 97.8 wt% quartz, 2.0 wt% tridymite, and 0.2 wt% calcite. Quantitative analysis of the surficial silica sample, P1-85, confirmed the crystallinity to be amorphous silica with 96.0 wt% as amorphous, 3.8 wt% as calcite, and only 0.2 wt% as quartz. The quantitative analysis of sample 7a, taken mid-way from the surface and sample 7b of a paleospring, showed an intermediate silica crystallinity with 62.0 wt% amorphous, 12.6 wt% cristobalite, 11.4 wt % calcite, 8.6 wt% tridymite, and 5.6 wt% quartz.

Figure 12: SEM images and corresponding XRD analyses of samples from the Puchuldiza geothermal field. a) Sample P84. Silicified microbial life is seen from SEM imagery. XRD analyses show amorphous silica as the predominant mineral. Calcite was also present but would have been removed during HCl cleaning before isotopic analysis. b) SEM image of paleosinter sample 7a. The small platelets are Opal-CT as depicted from the XRD analysis to the left. Once again, a large calcite peak is also shown in the XRD image but calcite would have been removed during HCl treatment. c) SEM image of paleosinter sample 7b depicting microcrystalline quartz growing in and around holes in the sample. The XRD analysis to the left shows clear quartz peaks with very little contamination.

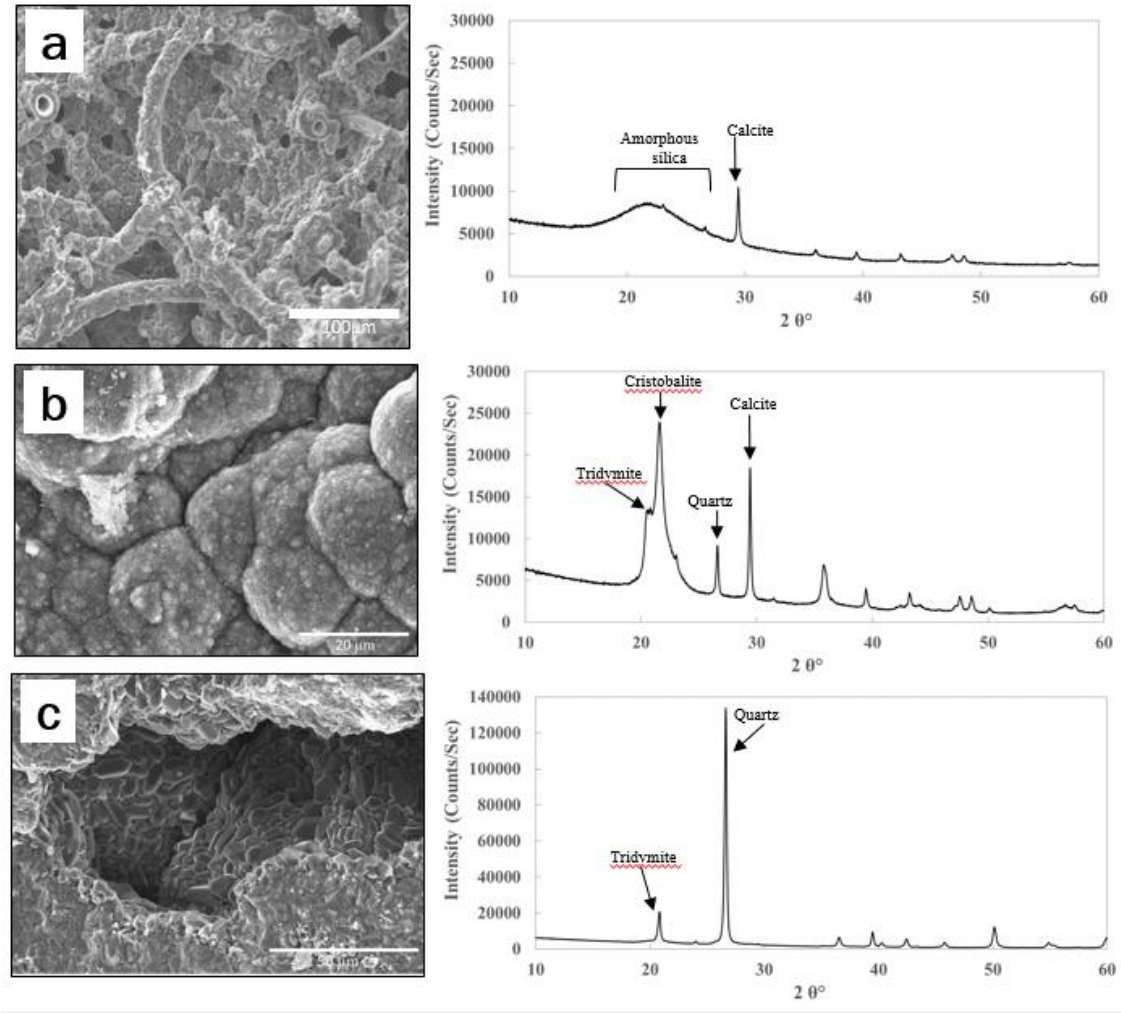

Table 1: Temperature and pH of each of the three sample sites from the Puchuldiza hot spring. Temperature and pH was measured 4 times at different times of day to track how temperature or pH may fluctuate on a daily basis.

	Day 1 (Plate Installation)				Day 4				Day 5				Day 9 (Plate Removal)			
	Time	Air T (°C)	Water T (°C)	pH	Time	Air T (°C)	Water T (°C)	pH	Time	Air T (°C)	Water T (°C)	pH	Time	Air T (°C)	Water T (°C)	pH
Site 1	3:30 PM	20.0	84.6	8.57	9:50 AM	14.1	82.3	8.55	7:15 AM	1.2	83.2	8.56	3:15 PM	18.1	81.4	8.68
Site 2	3:30 PM	20.0	70.3	8.80	9:50 AM	14.1	73.8	8.70	7:15 AM	1.2	72.9	8.64	3:15 PM	18.1	71.7	8.71
Site 3	3:30 PM	20.0	63.2	8.72	9:50 AM	14.1	64.8	8.72	7:15 AM	1.2	67.3	8.55	3:15 PM	18.1	62.3	8.67

Neither temperature nor pH varied by more than 5°C and 0.1, respectively, between all measuring instances (Table 1). The average pH of the hot spring source was 8.59 and the average temperature was 82.9°C. Away from the source, the average pH generally became more basic (around 8.7, Table 1). The pH does not appreciably affect silica solubility below a pH of 9.8 (Alexander et al., 1954), suggesting pH variation is not responsible for silica precipitation. The $\delta^{18}O$ value of the hot spring waters plot about 2‰ heavier than the reported $\delta^{18}O$ value of meteoric water from a stream in the geothermal field but plot within the range of δD values, indicating water-rock interaction of the geothermal water (Mahon and Cusicanqui, 1980; Horita and Wesolowski, 1994; Fig. 8). The $\delta^{18}O$ and δD values of the condensed steam plot on an evaporation trend from the isotopic composition of the geothermal water with a slope of 5.6 at ~85ºC (Mahon and Cusicanqui, 1980; Fig. 8).

Water samples from the hot spring showed similar $\delta'^{18}O$ values regardless of temperature. Water was sampled twice at each sampling location, once at the beginning of the field work and once at the end, to track oxygen isotope variability over the 9 days of field work. Water from the spring's source had an average $\delta'^{18}O$ value of -10.73‰ and varied by 0.85‰ between the first and last water sampling instance. The water sampled farthest from the source (around 63°C) showed the largest variation in $\delta'^{18}O$

Figure 13: Graph of the Chilean samples and water in $\Delta'^{17}O$-$\delta'^{18}O$ space with the single mineral thermometer fractionation line (Sharp et al., 2016). Samples plot on or very close to the fractionation line, indicating equilibrium processes. Green triangles are the formation waters. Green circles are amorphous silica formed on the surface, yellow circle is the silica precipitated from the steam condensate with the yellow triangle the corresponding steam condensate, red circles are the paleosinter samples, error bars are indicate the reported uncertainty.

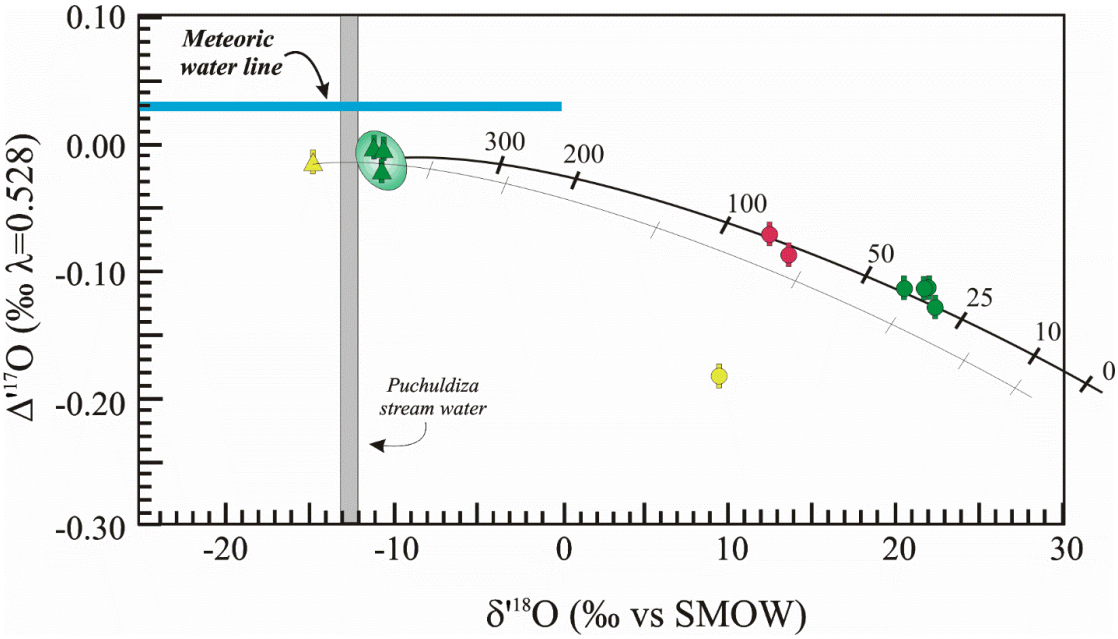

values with a 2.4‰ change between the first and last water sampling instance, suggesting that environmental factors such as evaporation could affect water samples further from the spring source. However, the average $\delta'^{18}O$ value (-10.53‰) at the 63°C location was similar to the other sampling sites (Appendix III). The $\Delta'^{17}O$ values of the water samples did not follow what is expected during evaporation where the $\Delta'^{17}O$ values decrease with more evaporation. The average $\Delta'^{17}O$ values of hot spring waters were -0.023‰ at the source and -0.009‰ at the water samples in the source's runoff channel (samples 63.2W, 62.3W, 70.3W, and 71.7 W, Appendix III). The water condensed from steam (sample 7eW) showed evaporation trends with the most negative $\delta'^{18}O$ value (-15.29‰) and a $\Delta'^{17}O$ value of -0.012‰ (Appendix III).

Figure 14: Example of glass microscope slide with precipitated silica placed in 70°C water for 9 days. All silica was precipitated above the water line (depicted).

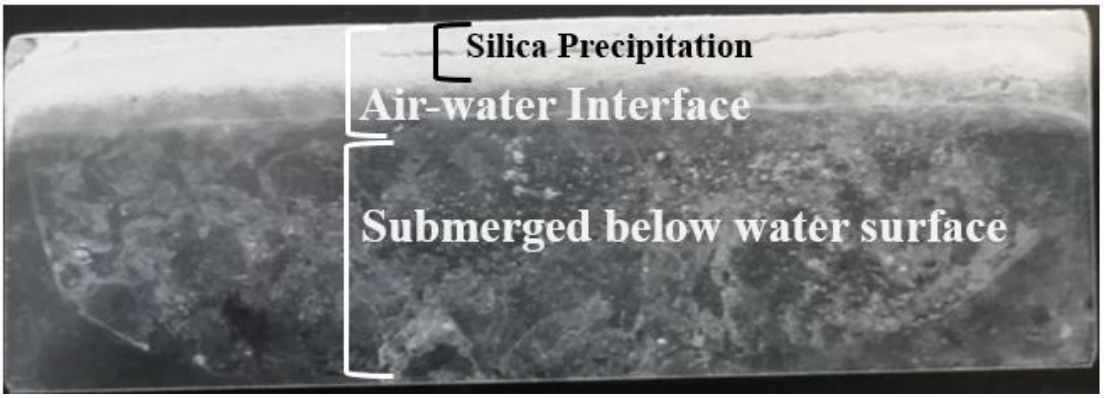

The $\Delta'^{17}O$-$\delta'^{18}O$ values of the all samples collected from the Puchuldiza geothermal system are plotted in Figure 13. The surficial amorphous silica samples plot in equilibrium with the formation waters but at much lower temperatures than the measured water temperatures. In contrast, the $\Delta'^{17}O$-$\delta'^{18}O$ values of the paleosinter samples, which have recrystallized below the surface to more stable silica phases, record temperatures that are very similar to the measured water temperatures. Either the modern, amorphous silica form out of equilibrium with the water, or they form at significantly lower temperatures than those suggested by the water temperature. Equations 5 and 6 estimated temperatures that varied within 0.5°C between each equation but were well below the measured temperatures of the water. Estimated temperatures ranged between 37.7ºC and 45.7ºC with no trend corresponding to the measured water temperature. Expectedly, equation 7 produces more variable temperatures but were all still well below the measured temperatures in the active hot spring.

Glass microscope slides were left for 9 days at each water sampling location in the active hot spring in order to collect freshly precipitated silica. The only glass microscope slide that contained enough silica to analyze was from the sampling location

corresponding with a 70ºC temperature (sample Plate-70). Precipitation only occurred at and above the air-water interface and not sub-aerially (Fig. 14). The silica sample from Plate-70 has a $\delta'^{18}O$ value that is 2‰ lighter and a $\Delta'^{17}O$ value that is 0.014‰ heavier than the bulk sinter sample taken at the 70ºC sample site (sample P70), resulting in a temperature estimate 8ºC warmer than sample P70 (Appendix III). If seasonality was the driving factor of precipitation, the $\delta'^{18}O$ value of the sinter would have to decrease by over 10‰ or the $\delta'^{18}O$ of the water would have to increase by 10‰ for equations 5 and 6 to estimate temperatures closer to the measured water temperatures. This does not seem likely, suggesting another factor is affecting the silica-water fractionation in the hot spring.

The $\Delta'^{17}O$-$\delta'^{18}O$ values of the silica precipitating with the steam (sample 7e) and the corresponding condensed water sample (sample 7eW) do not plot in triple oxygen isotopic equilibrium (Fig. 13). A calculated temperature of silica formation using equations 5 and 6 is 78°C versus a measured temperature of 88°C. However the sample does appear to be in equilibrium, resulting in a very different temperature estimate using equation 7 (14°C, Appendix III). The θ value of this sample is 0.5217, also suggesting non-equilibrium (Luz et al., 1999; Fig. 15).

The oxygen isotopic values of the paleosinter samples (7a and 7b) resulted in estimated temperatures closer to the measured temperatures at the source of the hot spring and appear to be in equilibrium with the modern water when plotted in $\Delta'^{17}O$-$\delta'^{18}O$ space (Appendix III, Fig. 13). Calculated temperatures from equations 5 and 6 suggests a formation temperature of 82°C and 89°C for samples 7a and 7b, respectively. As with the other samples of this study, temperature estimates using equation 7 were much more

variable (Appendix III). Temperature of an active fumarole within 0.5 meters of the paleosinter had a temperature of 88.1ºC

The θ-T values of the amorphous silica samples (samples P84, P70, and P63) plot in excellent agreement with the best fit of the data from Sharp et al. (2016) when using the estimated temperatures but does not fit well using the measured temperatures (Fig. 15). The paleosinter (samples 7a and 7b) plot in excellent agreement with the data from Sharp et al. (2016) in θ-T space when using the calculated temperature of formation (Fig. 15). Assuming the calculated temperatures are more realistic than the measured temperatures, the equation for the best fit line is identical to equation 8 but with a lower, but still significant, R^2 value of 0.98 and a higher error for the x-variable constant (1.81 ±0.13).

Figure 15: Graph depicting θ vs temperature. Data from Cao and Liu (2011) is in dark grey triangles, data from Sharp et al. (2016) is in light grey squares, and the Puchuldiza samples of this study in color. Large, dark green circles are the measured temperatures from the active hot spring. Smaller, lighter green cricles are the calculated temperatures using equation 5. The light red circles are the paleosinter samples (7a and 7b) calculated temperatures using equation 5. These plot in excellent agreement with the best fit from the study by Sharp et al. (2016). The yellow circles are the measured and calculated temperatures of sample 7e and do not plot near expected equilibrium values.

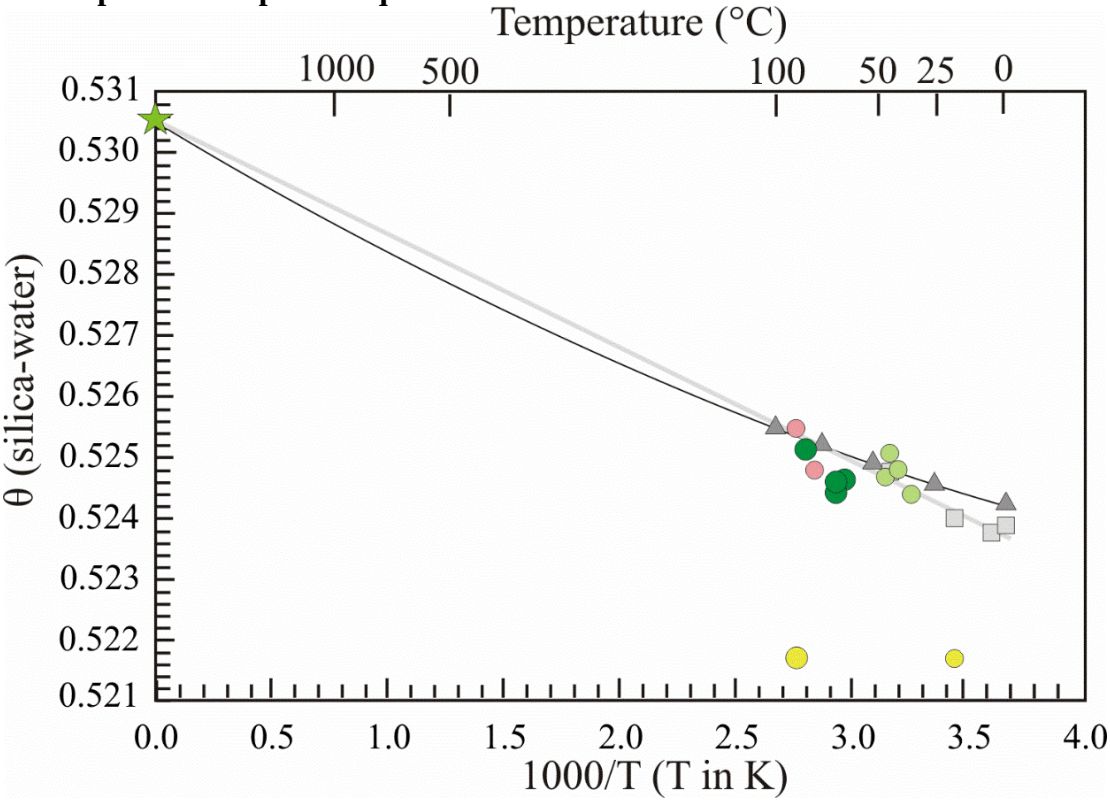

DISCUSSION

Iceland:

Water could only be sampled before and after the heat exchanger, at 57°C and 118°C, due to sampling limitations. Although the heat exchanger has a large, 3384 m^2, surface area to cool the water from 118°C to 60°C (Hallgrímsdóttir et al., 2012), the geothermal power plant is a closed system and the isotopic composition of the water did not change significantly between the two temperatures, as expected (Appendix II). The heavier $\delta^{18}O$ values of the geothermal water compared to cold water of the region are probably due to basalt-water mixing. Since the elemental concentration of hydrogen in the bedrock is extremely low compared to that of oxygen, the oxygen, but not hydrogen, isotope values of the water changes (Taylor, 1978). The hydrogen isotope value of the water from the Hellisheiði power plant is nearly unaltered, compared to meteoric water of the region (Fig. 8). Similarly, the triple oxygen isotopic composition of the water samples do not plot within the triple oxygen isotopic range of currently measured meteoric waters (Luz and Barkan, 2010). High temperature interaction with basalt caused the $\delta^{18}O$ values of the water to increase (Hattori and Muehlenbachs, 1982). The meteoric water near the Hellisheiði power plant has a $\delta^{18}O$ value of -8.0‰ to -9.0‰ (Mutonga, 2007) while the Icelandic bedrock (primarily Mid-Ocean Ridge Basalt, MORB) has a $\delta^{18}O$ value of ~5‰ (Hattori and Muehlenbachs, 1982). Meteoric water has an average $\Delta'^{17}O$ value of 0.03‰ (Luz and Barkan, 2010) while MORB is -0.005‰ (Herwartz et al., 2015; Sharp et al., 2016). Using a mixing model, the water appears to be 20% altered after the high temperatures and broad, diffuse pathways that the water travels before the heat exchanger (Appendix IV).

Temperature estimates from equations 5, 6, and 7 provides a range of accuracy when compared to the measured temperatures in which the silica precipitated. If the equations had a systematic bias, the temperature estimates would all be offset in the same sense – either higher or lower than the measured temperatures. However, the 118°C sample from this study was underestimated by 6.7°C, less than the 100°C and 85°C samples. Equation 7 has a much larger uncertainty associated with the temperature measurements but can be used as a tool to suggest non-equilibrium processes better than $\delta^{18}O$ measurements alone.

The $1000\ln\alpha^{18}O_{silica\text{-}water}$ versus $10^6/T^2$ values of the high and low temperature samples are in agreement with the published fractionation values from the literature (Sharp et al., 2016 and studies therein; Fig. 16). The samples from within the heat exchanger plot above the best fit line in $1000\ln\alpha^{18}O_{silica\text{-}water}$-$10^6/T^2$ space, probably due to an overestimation of the temperatures in the heat exchanger at the sites where the samples were collected. Silica-water fractionation of silica precipitating in a geothermal plant in Japan was measured by Kita et al. (1985). The $1000\ln\alpha^{18}O_{silica\text{-}water}$ value of the 60°C sample is only 0.13 different from the same temperature in the Kita et al. (1985) study. This is the only temperature that overlaps the data from Kita et al. (1985) and can be directly compared.

In accordance to the Cao and Liu (2011) and Sharp et al. (2016) studies, the θ value of a silica-water pair should be lower with lower temperatures (Fig. 11). Over the temperature range from 118-60°C the θ should change from 0.5258 to 0.5248 in accordance to the best fit from Sharp et al. (2016) and 0.5251 to 0.5258 in accordance to the best fit from Cao and Liu (2011). The θ value changed from 0.5252 at 60ºC to 0.5257

Figure 16: Reproduction of $1000ln\alpha^{18}_{qz\text{-}wt}$ vs. measured temperature ($10^6/T^2$) using the calibration of Sharp et al. (2016 and references therein). The data from Icelandic silica scale is plotted (blue diamonds) for comparison. The temperature of formation appears to be overestimated for the 100°C and 85ºC samples. Yellow circles are the data from the samples in the study by Sharp et al. (2016). Red circles are the data from the samples in the study by Kita et al. (1985). (adapted from Sharp et al., 2016)

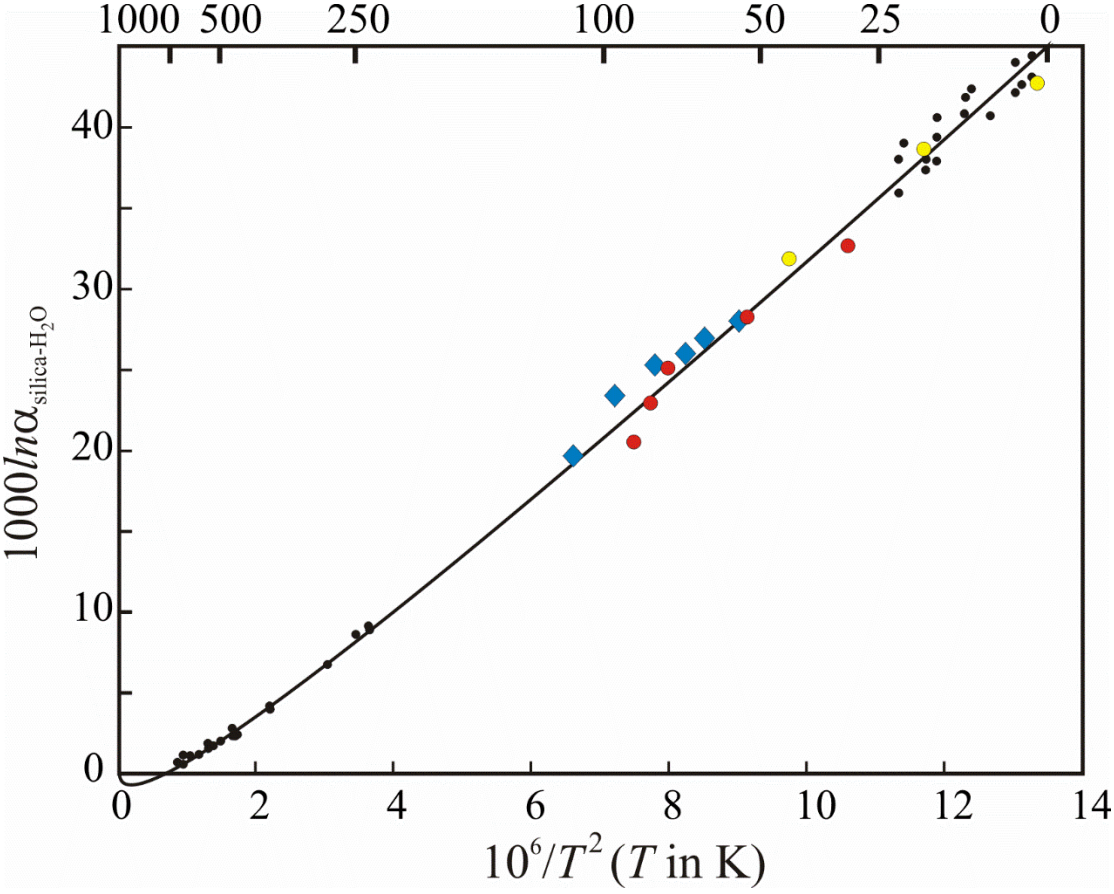

at 118ºC, a difference of 0.0005 (Fig. 11, Appendix II), suggesting the data from this study are in slightly better agreement with the best fit from Cao and Liu (2011) but within error of similar θ determinations from Sharp et al. (2016). The temperature interval of this study is in a range where the best fit lines from the data of both Cao and Liu (2011) and Sharp et al. (2016) intersect, prohibiting any definitive conclusions between the θ-T variations of biogenic vs. abiogenic silica-water fractionation.

Chile:

The isotopic values of surficial sinter samples from the active hot spring (samples P85, P70, P63, and Plate-70) plot in triple oxygen isotopic equilibrium with their formation waters, although the oxygen isotopic fractionations suggest equilibration temperatures far lower than the measured water temperatures (Fig. 13). The temperature gradient of the water away from the spring's source did not change drastically during the study period. The water temperature measurement made during the coldest part of the day (1.2°C air temperature) was 1-2°C warmer than when measured later in the day when the air temperature was 18-20°C (Table 1). The lower temperature estimates suggest that the sinter is not precipitating at the temperature measured in the water but does precipitate between 38-46°C, driven by near-surface evaporation and/or cooling. The glass microscope slides that were left in the hot spring to collect fresh precipitation support this conclusion. No silica precipitation occurred on the slides below the surface of the water. Silica only precipitated at the air-water interface (AWI) (Fig. 14). Silica precipitation at the AWI is in agreement with findings in the studies by Tobler et al. (2008) and Mountain et al. (2003) where hot spring water that were slightly basic and under-saturated with respect to silica had low subaqueous precipitation and the primary drivers of precipitation were evaporation and/or cooling.

High evaporation rates are expected in the dry climate of the Chilean Altiplano. The evaporation fractionation trend ($\theta = 0.529$; Barkan and Luz, 2005) would shift the waters to higher $\Delta'^{17}O$ and $\delta'^{18}O$ values, which could not be in equilibrium with the silica at any temperatures (Appendix V). However, decreasing temperature drives the water towards saturation with respect to silica and is in very good agreement with the calculated

temperature of formation based on the oxygen isotopic data for these samples. Temperatures between 22ºC and 50ºC are necessary to precipitate silica in waters with the silica concentration range found in the Puchuldiza geothermal system, 110-186 ppm (Fig. 17). The formation temperatures suggested by the triple oxygen isotopic composition of the amorphous silica fall exactly in this range (Fig. 17). Therefore, the triple oxygen isotopic value of the precipitated sinter suggests that the silica formed in

Figure 17: Graph showing silica saturation line from the literature (Fournier and Rowe, 1966) along with the silica concentration in the source waters from the Puchuldiza hot springs (red circles). Silica precipitation would not occur in the spring until the temperature of the water cools to the silica saturation line (blue circle).

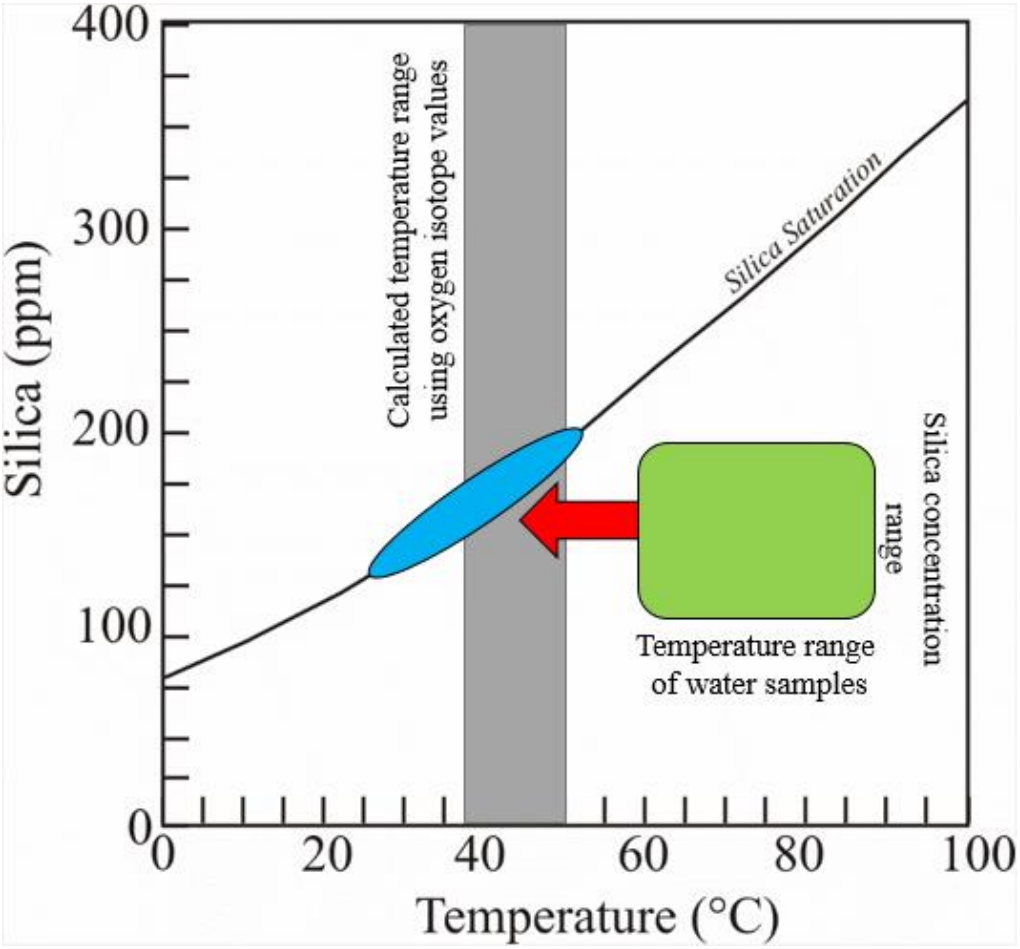

equilibrium with the formation water and the oxygen isotopic values suggest that the typical temperature of the residual water when it reaches supersaturation is between 38-46°C in the Puchuldiza geothermal field.

The freshly precipitated sinter (sample 7e) that formed from the steam condensate (7eW) was not in equilibrium with the water that was collected from the steam (Fig. 13). However, the estimated temperature using equations 5 and 6 were close to the measured temperature of the steam (88.1°C). Only the $\Delta'^{17}O$ value of the sinter shows that the silica is clearly not in equilibrium (Fig. 13). A difference in $1000\ln\alpha_{silica\text{-}water}$ for oxygen-17 or oxygen-18 values for samples not in equilibrium does not result in a large difference in the temperature estimation. The differences are easier to see in $\Delta'^{17}O$ values where a 0.1‰ change is much larger.

The paleosinter is more crystalline than the newly-precipitated surficial silica, suggesting that the amorphous silica has undergone diagenesis after burial (Lynne et al., 2005). The triple oxygen isotope measurements of the paleosinter (samples 7a and 7b) suggest that the sinter formed in equilibrium or more likely re-equilibrated as they recrystallized to quartz at the maximum measured temperature of the hot springs (Fig. 13). The paleosinter was obtained from an active fumarole, close to a region where sinter was actively forming from the fumarolic steam. Diagenesis can occur in as little as 21 weeks when exposed to acidic steam (Lynne et al., 2006). However the paleosinter measured is unlikely to have re-equilibrated with the fumarolic steam condensate because the re-precipitated silica (sample 7e) is not in equilibrium (Fig. 13). Therefore, the paleosinter probably recrystallized in equilibrium below the surface at near-boiling conditions, preserving the highest temperature of the hot spring.

CONCLUSION

The triple oxygen isotope values of silica scale and coexisting water from the geothermal plant in Iceland confirm the θ-temperature relationships of Cao and Liu (2011) and Sharp et al. (2016). Using the triple isotope system, the silica scale appears to be in equilibrium with the formation water at the measured temperature locations. The intermediate temperatures from inside the heat exchanger suggest a lower temperature of formation, likely due to an overestimation of temperature at the point at which the silica was taken. Nevertheless, we cannot exclude the possibilities that a) the neoform silica is not in equilibrium, and only fortuitously records a lower temperature, or b) that the amorphous silica-water fractionation equation is not the same as the quartz-water fractionation. This possibility is discounted, however, because the difference between the measured and calculated temperatures do not show a consistent offset one way or the other.

In the Puchuldiza hydrothermal springs, the amorphous silica precipitated at the surface appear to have formed in equilibrium with the formation water at a temperature between 38-50°C. Decreasing water temperature appears to be the primary driver for silica precipitation. The triple oxygen system suggests the paleosinter equilibrated with the hydrothermal water during diagenesis and preserved the near-boiling temperature of the hot spring. The $\Delta'^{17}O$ value of the sinter that precipitated in fumarolic steam condensate is not in equilibrium or some other factor resulted in a drastic lowering of the $\Delta'^{17}O$ value but could not be discerned from $\delta^{18}O$ values alone.

Paired $\delta'^{17}O$-$\delta'^{18}O$ measurements can be used to accurately estimate the temperature of formation, the isotopic composition of the formation water, and most

importantly, discern between equilibrium and non-equilibrium processes. The silica-water thermometer appears to be valid for amorphous silica, opal CT and quartz. There does not appear to be any appreciable difference in the fractionation of water with either abiogenic or biogenic silica. Natural systems, such as geothermal fields, provide an excellent resource for further exploration on the effects that evaporation and temperature have on the triple oxygen isotope system and equilibrium silica-water fractionation.

APPENDICES

Appendix I **37**

Appendix II **39**

Appendix III **40**

Appendix IV **41**

Appendix V **42**

APPENDIX I:

Description of Samples:

118W – Water collected at 118°C from the Hellisheiði power plant, Iceland. Water was obtained through a valve in the pipe leading into the heat exchanger. Water is sampled after the steam has been separated for electricity production.

60W - Water collected at 60°C from the Hellisheiði power plant, Iceland. Water was obtained through a valve in the pipe leading out of the heat exchanger. Water is sampled before the steam and water are combined and injected back into the subsurface.

F.1 – Silica formed at 118°C from the Hellisheiði power plant, Iceland. Sample was collected in January of 2014 from the inlet pipe into the heat exchanger. Sample was collected after the steam is separated from the water.

F.2 – Silica formed at 100°C from the Hellisheiði power plant, Iceland. Sample was collected in January of 2014 from the heat exchanger during a routine cleaning procedure.

F.3 - Silica formed at 85°C from the Hellisheiði power plant, Iceland. Sample was collected in January of 2014 from the heat exchanger during a routine cleaning procedure.

R.10 – Silica formed at 75°C from the Hellisheiði power plant, Iceland. Sample was collected in January of 2014 from the heat exchanger during a routine cleaning procedure.

R.5 – Silica formed at 70°C from the Hellisheiði power plant, Iceland. Sample was collected in January of 2014 from the heat exchanger during a routine cleaning procedure.

R.9 – Silica formed at 60°C from the Hellisheiði power plant, Iceland. Sample was collected in January of 2014 from the outlet pipe leading out of the heat exchanger and before the steam and water are combined and injected back into the subsurface.

63.2W – Water collected at 63.2°C in a Puchuldiza hot spring, Chile (S19°24’24.2” W68°57’25.8”). Sample was collected on March 19, 2016.

70.3W – Water collected at 70.3°C in a Puchuldiza hot spring, Chile (S19°24’24.2” W68°57’25.8”). Sample was collected on March 19, 2016.

84.6W – Water collected at 84.6°C in a Puchuldiza hot spring, Chile (S19°24’24.2” W68°57’25.8”). Sample was collected on March 19, 2016.

62.3W – Water collected at 62.3°C in a Puchuldiza hot spring, Chile (S19°24’24.2” W68°57’25.8”). Sample was collected on March 28, 2016.

71.7W – Water collected at 62.3°C in a Puchuldiza hot spring, Chile (S19°24’24.2” W68°57’25.8”). Sample was collected on March 28, 2016.

81.4W – Water collected at 62.3°C in a Puchuldiza hot spring, Chile (S19°24’24.2” W68°57’25.8”). Sample was collected on March 28, 2016.

P84 – Sinter collected in a Puchuldiza hot spring, Chile (S19°24’24.2” W68°57’25.8”). Sample was collected on March 19, 2016. The measured temperature of the water running over the sample was 84.6°C.

P70 – Sinter collected in a Puchuldiza hot spring, Chile (S19°24’24.2” W68°57’25.8”). Sample was collected on March 19, 2016. The measured temperature of the water running over the sample was 70.3°C.

P63 – Sinter collected in a Puchuldiza hot spring, Chile (S19°24’24.2” W68°57’25.8”). Sample was collected on March 19, 2016. The measured temperature of the water running over the sample was 63.2°C.

7a – Paleosinter from an active fumarole from the Puchuldiza geothermal field, Chile (S19°24’47.3” W68°57’31.2”). The paleosinter is probably chalcedony as shown from the XRD spectra.

7b – Paleosinter from an active fumarole from the Puchuldiza geothermal field, Chile (S19°24’47.3” W68°57’31.2”). The paleosinter is probably microcrystalline quartz as shown from the XRD spectra.

7eW – Water condensed from a fumarole from the Puchuldiza geothermal field, Chile (S19°24’47.3” W68°57’31.2”). The measured temperature of the steam was 88.1°C.

7e – Fresh silica precipitated on a paleosinter located at the bottom of a fumarole in the Puchuldiza geothermal field, Chile (S19°24’47.3” W68°57’31.2”). The silica is assumed to have re-precipitated from the paleosinter as the steam dissolved and the outer layer of the rock.

Plate-70 – Fresh silica precipitated onto a microscope slide located in a hot spring over 9 days (from March 19, 2016 to March 28, 2016) at the Puchulidza geothermal field. The microscope slide was located in 70°C water.

APPENDIX II:

Compiled data of the water and silica samples from the Hellisheiði power plant in Iceland. All analyses were done at the University of New Mexico. All $\delta^{18}O$ and $\delta^{17}O$ values are reported relative to VSMOW. Bold numbers are the averages used in this study.

Sample	Sample Type	T (°C) Measured	$\delta^{17}O$	$\delta^{18}O$	$\delta'^{17}O$	$\delta'^{18}O$	$\Delta'^{17}O$ ($\theta = 0.528$)	θ (Calculated)	1000lnα ($^{17}O/^{16}O$)	1000lnα ($^{18}O/^{16}O$)	$\Delta'^{17}O$ (silica-water)	T (°C, Calc) $\delta'^{17}O$	T (°C, Calc) $\delta'^{18}O$	T (°C, Calc) $\Delta'^{17}O$
118W	Water	118	-3.21	-6.05	-3.21	-6.06	-0.010							
			-3.55	-6.66	-3.55	-6.69	-0.021							
		Average	**-3.38**	**-6.35**	**-3.38**	**-6.37**	**-0.015**							
60W	Water	60	-3.10	-5.85	-3.11	-5.86	-0.013							
			-3.16	-5.95	-3.17	-5.97	-0.014							
			-3.34	-6.30	-3.35	-6.31	-0.014							
		Average	**-3.20**	**-6.03**	**-3.21**	**-6.05**	**-0.014**							
F.1	Silica	118	6.83	13.09	6.81	13.01	-0.060	0.5257						
			7.34	14.00	7.31	13.96	-0.061	0.5258						
		Average	**7.09**	**13.55**	**7.06**	**13.48**	**-0.061**	**0.5257**	**10.439**	**19.857**	**-0.045**	**111.3**	**111.3**	**113.0**
F.2	Silica	100	8.69	16.66	8.65	16.52	-0.072	0.5255						
			8.91	17.11	8.87	16.96	-0.083	0.5251						
			9.35	17.97	9.22	17.62	-0.078	0.5254						
			9.25	17.72	9.20	17.57	-0.072	0.5256						
		Average	**9.05**	**17.36**	**8.99**	**17.17**	**-0.076**	**0.5254**	**12.369**	**23.541**	**-0.061**	**85.3**	**85.3**	**87.5**
F.3	Silica	85	10.27	19.71	10.22	19.52	-0.085	0.5252						
			10.35	19.85	10.29	19.65	-0.083	0.5253						
			10.45	20.05	10.40	19.85	-0.086	0.5253						
		Average	**10.36**	**19.87**	**10.30**	**19.67**	**-0.085**	**0.5253**	**13.511**	**25.723**	**-0.071**	**72.3**	**72.4**	**75.1**
R.10	Silica	75	10.58	20.29	10.52	20.09	-0.086	0.5252						
			10.41	19.95	10.36	19.75	-0.072	0.5257						
			10.65	20.43	10.59	20.23	-0.088	0.5252						
		Average	**10.54**	**20.22**	**10.49**	**20.02**	**-0.082**	**0.5254**	**13.698**	**26.072**	**-0.069**	**70.3**	**70.4**	**77.4**
R.5	Silica	70	11.24	21.54	11.17	21.31	-0.077	0.5257						
			10.95	21.03	10.89	20.81	-0.096	0.5249						
		Average	**11.09**	**21.28**	**11.03**	**21.06**	**-0.087**	**0.5253**	**14.240**	**27.108**	**-0.073**	**64.8**	**64.9**	**72.8**
R.9	Silica	60	11.35	21.77	11.28	21.53	-0.088	0.5253						
			11.87	22.78	11.796	22.521	-0.095	0.5252						
		Average	**11.61**	**22.27**	**11.54**	**22.03**	**-0.092**	**0.5253**	**14.747**	**28.077**	**-0.078**	**59.8**	**59.9**	**67.5**

APPENDIX III:

Compiled data of the water and silica samples from the Puchuldiza geothermal system in Chile. All analyses were done at the University of New Mexico. Bold lines are the averages used in this study. All $\delta^{18}O$ and $\delta^{17}O$ values are reported relative to VSMOW.

Sample	Sample Type	T (°C) Measured	$\delta^{17}O$	$\delta^{18}O$	$\delta'^{17}O$	$\delta'^{18}O$	$\Delta'^{17}O$ ($\theta = 0.528$)	θ (Calc.)	1000lnα ($^{17}O/^{16}O$)	1000lnα ($^{18}O/^{16}O$)	$\Delta'^{17}O$ (silica-water)	T (°C, Calc) $\delta'^{17}O$	T (°C, Calc) $\delta'^{18}O$	T (°C, Calc) $\Delta'^{17}O$
63.2W	Water	63.2	-6.16	-11.63	-6.18	-11.70	-0.001							
			-6.20	-11.69	-6.22	-11.76	-0.009							
		Average	**-6.18**	**-11.66**	**-6.20**	**-11.73**	**-0.005**							
62.3W	Water	62.3	**-4.93**	**-9.29**	**-4.94**	**-9.33**	**-0.012**							
70.3W	Water	70.3	**-5.44**	**-10.26**	**-5.46**	**-10.32**	**-0.009**							
71.7W	Water	71.7	**-5.66**	**-10.67**	**-5.67**	**-10.73**	**-0.009**							
84.5W	Water	84.5	**-5.67**	**-10.67**	**-5.69**	**-10.73**	**-0.023**							
81.4W	Water	81.4	**-5.22**	**-9.83**	**-5.24**	**-9.87**	**-0.022**							
P63	Silica	63.2	11.29	21.69	11.22	21.46	-0.105							
			12.15	23.37	12.07	23.10	-0.124							
			12.03	23.15	11.96	22.89	-0.123							
			11.34	21.79	11.27	21.56	-0.112							
		Average	**11.70**	**22.50**	**11.63**	**22.25**	**-0.116**	**0.5248**	**17.119**	**32.622**	**-0.105**	**39.3**	**39.4**	**44.0**
P70	Silica	70.3	11.76	22.70	11.69	22.44	-0.157							
			12.32	23.71	12.24	23.43	-0.129							
			11.41	21.90	11.34	21.66	-0.092							
		Average	**11.83**	**22.77**	**11.76**	**22.51**	**-0.126**	**0.5245**	**17.325**	**33.034**	**-0.117**	**37.7**	**37.7**	**35.6**
Plate-70	Fresh Silica	70.3	10.98	21.09	10.92	20.87	-0.100							
			10.85	20.88	10.79	20.67	-0.123							
			10.62	20.43	10.56	20.23	-0.115							
		Average	**10.82**	**20.80**	**10.76**	**20.59**	**-0.113**	**0.5247**	**16.323**	**31.110**	**-0.104**	**45.8**	**45.8**	**45.0**
P84	Silica	84.5	11.04	21.25	10.98	21.03	-0.121							
			11.81	22.70	11.74	22.45	-0.112							
			11.26	21.62	11.20	21.39	-0.094							
		Average	**11.37**	**21.86**	**11.31**	**21.62**	**-0.109**	**0.5251**	**16.954**	**32.286**	**-0.093**	**40.6**	**40.8**	**53.7**
7eW	Steam	88.1	**-8.05**	**-15.17**	**-8.09**	**-15.29**	**-0.012**							
7e	Silica	88.1	**4.80**	**9.44**	**4.79**	**9.39**	**-0.169**	**0.5217**	**12.876**	**24.683**	**-0.157**	**78.4**	**77.4**	**14.0**
7a	Paleosinter	NA	7.13	13.73	7.11	13.63	-0.092							
			7.084	13.625	7.05903	13.533	-0.086							
		Average	**7.11**	**13.68**	**7.08**	**13.58**	**-0.089**	**0.5248**	**12.614**	**24.034**	**-0.076**	**82.4**	**82.3**	**69.6**
7b	Paleosinter	NA	6.493	12.483	6.472	12.4057	-0.078							
			6.514	12.493	6.49288	12.4156	-0.063							
		Average	**6.50**	**12.49**	**6.48**	**12.41**	**-0.070**	**0.5255**	**12.014**	**22.862**	**-0.057**	**89.3**	**89.7**	**93.1**

APPENDIX IV:

Basalt-water mixing model:

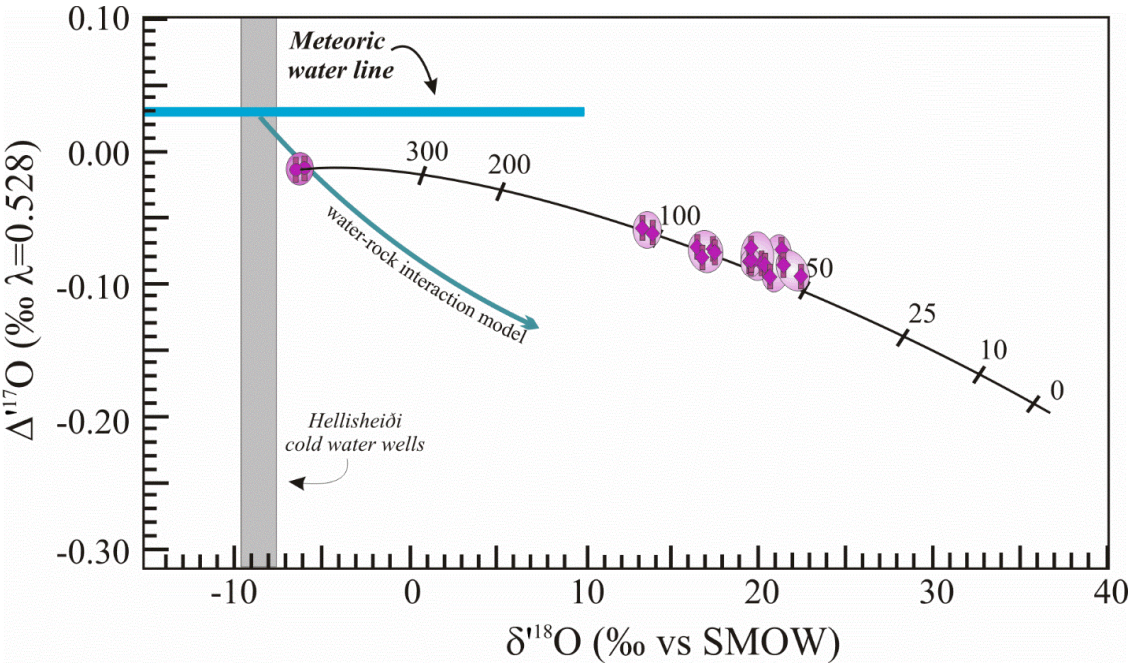

APPENDIX V:

An evaporation model for the effect on triple oxygen isotope equilibrium for silica-water fractionation. The slope of the evaporation trend line (light blue arrow) is 0.529 (Barkan and Luz, 2005). Silica samples would have to plot on the red dotted line to be in equilibrium with evaporated hot spring water.

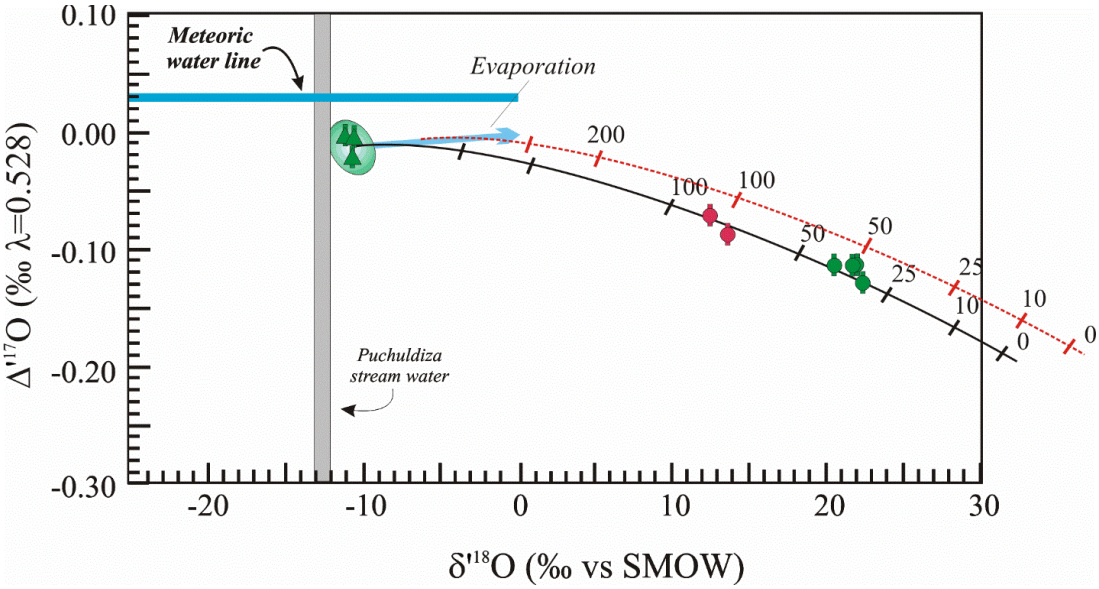

REFERENCES:

Alexander, G. H., W.; Iler, R., 1954, The Solubility of Amorphous Silica in Water: The Journal of Physical Chemistry, v. 58, no. 6, p. 453-455.

Amjad, Z. and Zuhl, R., 2008, An evaluation of silica scale control additives for industrial water systems, CORROSION Conference & Expo: Houston, Texas, USA, NACE International, p. Paper No. 08368.

Aramaki, Y. Y., Takushi; Okaue, Yoshihiro; Imai, Akira; Watanabe, Koichiro 2005, A Study on the Formation of Smectite in Silica Scales Precipitated from Geothermal Water: The Effect of Magnesium: Resource Geology, v. 55, no. 3, p. 281-284.

Arnórsson, S., 1975, Application of the silica geothermometer in low temperature hydrothermal areas of Iceland: American Journal of Science, v. 275, p. 763-784.

Barkan, E., and Luz, B., 2005, High precision measurements of 17O/16O and 18O/16O ratios in H2O: Rapid Commun Mass Spectrom, v. 19, no. 24, p. 3737-3742.

Cady, S., Farmer, J., 1996, Fossilization processes in siliceous thermal springs: trends in preservation along thermal gradients, in Proceedings CIBA Foundation Symposium, Wiley, Chichester, U.K, p. 150-173.

Campbell, K. A., Sannazzaro, K., Browne, P. L. R., Herdianita, N. R., and Rodgers, K. A., 2001, Sedimentary facies and mineralogy of the Late Pleistocene Umukuri silica sinter, Taupo Volcanic Zone, New Zealand: Journal Of Sedimentary Research Section A And B, v. 71, no. Part 5, p. 727-746.

Cao, X., and Liu, Y., 2011, Equilibrium mass-dependent fractionation relationships for triple oxygen isotopes: Geochimica et Cosmochimica Acta, v. 75, no. 23, p. 7435-7445.

Clayton R. N., Grossman L., and Mayeda T. K. (1973) A component of primitive nuclear composition in carbonaceous meteorites. Science 182, 485-488.

Clayton, R. N., 1993, Oxygen Isotopes in Meteorites: Annual Reviews Earth and Planetary Science, v. 21, p. 115-149.

Craig, H., Gordon, L., 1965, Deuterium and oxygen 18 variations in the ocean and the marine atmosphere: In proc. Stable Isotopes in Oceanographic Studies and Paleotemperatures, p. 9-130.

Dodd, J. P., and Sharp, Z. D., 2010, A laser fluorination method for oxygen isotope analysis of biogenic silica and a new oxygen isotope calibration of modern diatoms in freshwater environments: Geochimica et Cosmochimica Acta, v. 74, no. 4, p. 1381-1390.

Fleming, B., and Crerar, D., 1982, Silicic acid ionization and calculation of silica solubility at elevated temperature and pH application to geothermal fluid processing and reinjection: Geothermics, v. 11, no. 1, p. 15-29.

Fournier, R. Rowe, J., 1966, Estimation of underground temperatures from the silica content of water from hot springs and wet-steam wells: American Journal of Science, v. 264, p. 695-697.

Franzson, H. K., Bjarni Reyr; Gunnarsson, Gunnar; Björnsson, Grímur; Hjartarson, Arnar; , and Steingrímsson, B. G., Einar; Gíslason, Gestur The Hengill-Hellisheiði Geothermal Field. Development of a Conceptual Geothermal Model, in Proceedings Proceedings World Geothermal Congress, Antalya, Turkey, 2005.

Gallup, D. L., 2002, Investigations of organic inhibitors for silica scale control in geothermal brines: Geothermics, v. 31, p. 415-430.

Gallup, D. L., and Barcelon, E., 2005, Investigations of organic inhibitors for silica scale control from geothermal brines–II: Geothermics, v. 34, no. 6, p. 756-771.

Garcia-Valles, M., Fernandez-Turiel, J. L., Gimeno-Torrente, D., Saavedra-Alonso, J., and Martinez-Manent, S., 2008, Mineralogical characterization of silica sinters from the El Tatio geothermal field, Chile: American Mineralogist, v. 93, no. 8-9, p. 1373-1383.

Geilert, S., Vroon, P. Z., Keller, N. S., Gudbrandsson, S., Stefánsson, A., and van Bergen, M. J., 2015, Silicon isotope fractionation during silica precipitation from hot-spring waters: Evidence from the Geysir geothermal field, Iceland: Geochimica et Cosmochimica Acta, v. 164, p. 403-427.

Giggenbach, W. F., 1978, The isotopic composition of waters from the El Tatio geothermal field, Northern Chile: Geochimica et Cosmochimica Acta, v. 42, no. 7, p. 979-988.

Guidry, S. Chaftez, H., 2002, Factors governing subaqueous siliceous sinter precipitation in hot springs: examples from Yellowstone National Park, USA: Sedimentology, v. 49, p. 1253-1267.

Gunnarsson, I. and Arnorsson, S., 2002, Amorphous silica solubility and the thermodynamic properties of H4SiO4º in the range of 0º to 350ºC at Psat: Geochimica et Cosmochimica Acta, v. 64, p. 2295-2307.

Hallgrímsdóttir, E. B., Claus; Hrólfsson, Ingólfur 2012, The Geothermal Power Plant at Hellisheiði, Iceland: GRC Transactions, v. 36, p. 1067-1072.

Harrar, J., Locke, F., Otto, C.H., Jr., Lorensen, L., Monaco, S. and Frey, W., 1982, Field tests of organic additives for scale control at the Salton Sea geothermal field: Old SPE Journal, v. 22, p. 17-27.

Hattori, K., and Muehlenbachs, K., 1982, Oxygen isotope ratios of the Icelandic crust: Journal of Geophysical Research: Solid Earth, v. 87, no. B8, p. 6559-6565.

Hayashi, K., 2013, Oxygen Isotope Study of Silica Sinter from the Osorezan Geothermal Field, Northeast Japan: International Journal of Geosciences, v. 04, no. 10, p. 1438-1446.

Henley, R., 1983, pH and silica scaling control in geothermal field development: Geothermics, v. 12, no. 4, p. 307-321.

Herdianita, N. R., Browne., P.R.L, Rodgers, K.A, Campbell, K.A, 2000, Mineralogical and textural changes accompanying ageing of silica sinter: Mineralium Deposita, v. 35, p. 48-62.

Herwartz, D., Pack, A., Krylov, D., Xiao, Y., Muehlenbachs, K., Sengupta, S., and Di Rocco, T., 2015, Revealing the climate of snowball Earth from Delta17O systematics of hydrothermal rocks: Proc Natl Acad Sci U S A, v. 112, no. 17, p. 5337-5341.

Horita, J. Wesolowski, D., 1994, Liquid-vapor fractionation of oxygen and hydrogen isotopes of water from the freezing to the critical temperature: Geochimica et Cosmochimica Acta, v. 58, no. 16, p. 3425-3437.

Inagaki, F., Motomura, Y., and Ogata, S., 2003, Microbial silica deposition in geothermal hot waters: Appl Microbiol Biotechnol, v. 60, no. 6, p. 605-611.

Jones, B., Renaut, R. W., and Rosen, M. R., 2000, Stromatolites Forming in Acidic Hot-Spring Waters, North Island, New Zealand: Palaios, v. 15, no. 5, p. 450-475.

Kita, I. Taguchi, S., Matsubaya, O., 1985, Oxygen isotope fractionation between amorphous silica and water at 34-93 degrees C: Nature, v. 314, no. 7, p. 83-84.

Lahsen, A., Sepúlveda, F., Rojas, J., Palacios, C., 2005, Present Status of Geothermal Exploration in Chile, Proceedings World Geothermal Congress: Antalya, Turkey.

Li, S., Passey, B., Henkes G, Levin, N., 2016, Triple Oxygen and Clumped Isotope Equilibrium Fractionation in Synthetic Carbonate-Water Systems. 2016 Annual Goldschmidt Conference. Yokohama, Japan.

Luz, B. B., E.; Bender, M.; Thiemens, M.; Boering, K., 1999, Triple-isotope composition of atmospheric oxygen as a tracer of biosphere productivity: Nature, v. 400, p. 547-550.

Luz, B., Barkan, L., 2010, Variations of 17O/16O and 18O/16O in meteoric waters: Geochimica et Cosmochimica Acta, v. 74, no. 22, p. 6276-6286.

Lynne, B. Campbell, K., 2004, Morphologic and mineralogic transitions from opal-a to opal-ct in low-temperature siliceous sinter diagenesis, Taupo volcanic zone, New Zealand: Journal of sedimentary research, v. 74, no. 4, p. 561-579.

Lynne, B. Y., 2012, Mapping vent to distal-apron hot spring paleo-flow pathways using siliceous sinter architecture: Geothermics, v. 43, p. 3-24.

Lynne, B. Y., and Campbell, K. A., 2003, Diagenetic transformations (opal-A to quartz) of low- and mid-temperature microbial textures in siliceous hot-spring deposits, Taupo Volcanic Zone, New Zealand: Canadian Journal of Earth Sciences, v. 40, no. 11, p. 1679-1696.

Lynne, B. Y., Campbell, K. A., James, B. J., Browne, P. R. L., and Moore, J., 2007, Tracking crystallinity in siliceous hot-spring deposits: American Journal of Science, v. 307, no. 3, p. 612-641.

Lynne, B. Y., Campbell, K. A., Moore, J., and Browne, P. R. L., 2008, Origin and evolution of the Steamboat Springs siliceous sinter deposit, Nevada, U.S.A: Sedimentary Geology, v. 210, no. 3-4, p. 111-131.

Lynne, B. Y., Campbell, K. A., Moore, J. N., and Browne, P. R. L., 2005, Diagenesis of 1900-year-old siliceous sinter (opal-A to quartz) at Opal Mound, Roosevelt Hot Springs, Utah, U.S.A: Sedimentary Geology, v. 179, no. 3-4, p. 249-278.

Lynne, B. Y., Campbell, K. A., Perry, R. S., Browne, P. R. L., and Moore, J. N., 2006, Acceleration of sinter diagenesis in an active fumarole, Taupo volcanic zone, New Zealand: Geology, v. 34, no. 9, p. 749.

Mahon, W. A. J., Cusicanqui, H., 1980, Geochemistry of the Puchuldiza and Tuja hot springs, Chile: New Zealand Journal of Science, v. 23, p. 149-159.

Matsuhisa, Y., Goldsmith, J. R., and Clayton, R. N., 1978, Mechanisms of hydrothermal crystallization of quartz at 250°C and 15 kbar: Geochimica et Cosmochimica Acta, v. 42, no. 2, p. 173-182.

Meier, D. B., Gunnlaugsson, E., Gunnarsson, I., Jamtveit, B., Peacock, C. L., and Benning, L. G., 2014, Microstructural and chemical variation in silica-rich precipitates at the Hellisheiði geothermal power plant: Mineralogical Magazine, v. 78, no. 6, p. 1381-1389.

Miller, M. F., 2002, Isotopic fractionation and the quantification of 17O anomalies in the oxygen three-isotope system: an appraisal and geochemical significance: Geochimica et Cosmochimica Acta, v. 66, no. 11.

Mountain, B. W., Benning, L. G., and Boerema, J. A., 2003, Experimental studies on New Zealand hot spring sinters: rates of growth and textural development: Canadian Journal of Earth Sciences, v. 40, no. 11, p. 1643-1667.

Murata, K. J. Friedman, I., Gleason, J.D 1977, Oxygen isotope relations between diagenetic silica minerals in Monterey Shale, Temblor Range, California: American Journal of Science, v. 277, p. 259-272.

Mutonga, M. W., 2007, The Isotopic And Chemical Characteristics Of Geothermal Fluids In Hengill Area, Sw-Iceland: Hellisheiði, Hveragerdi And Nesjavellir Fields: United Nations University.

Nicolau, C., 2013, Physico-Chemical And Environmental Controls On Siliceous Sinter Formation At The High-Altitude El Tatio Geothermal Field, Northern Chile Master's of Science: Universidad de Chile, 45 p.

Nicolau, C., Reich, M., and Lynne, B., 2014, Physico-chemical and environmental controls on siliceous sinter formation at the high-altitude El Tatio geothermal field, Chile: Journal of Volcanology and Geothermal Research, v. 282, p. 60-76.

O'Neil J. R. and Epstein S., 1966, A method for oxygen isotope analysis of milligram quantities of water and some of its applications. J. Geophys. Res. 71, 4955–4961.

Pack, A., and Herwartz, D., 2014, The triple oxygen isotope composition of the Earth mantle and understanding variations in terrestrial rocks and minerals: Earth and Planetary Science Letters, v. 390, p. 138-145.

Pambudi, N. A., Itoi, R., Yamashiro, R., Css Syah Alam, B. Y., Tusara, L., Jalilinasrabady, S., and Khasani, J., 2015, The behavior of silica in geothermal brine from Dieng geothermal power plant, Indonesia: Geothermics, v. 54, p. 109-114.

Pope, E. C., Bird, D. K., Arnórsson, S., and Giroud, N., 2016, Hydrogeology of the Krafla geothermal system, northeast Iceland: Geofluids, v. 16, no. 1, p. 175-197.

Pope, E. C., Bird, D., Arnórsson, S., Fridriksson, T., Elders, W.A., Fridleifsson, G.Ó. Iceland Deep Drilling Project (IDDP): Stable Isotope Evidence of Fluid Evolution in Icelandic Geothermal Systems, in Proceedings Proceedings World Geothermal Congeress, Bali, Indonesia, 2010, p. 25-29.

Rodgers, K. A., Browne, P. R. L., Buddle, T. F., Cook, K. L., Greatrex, R. A., Hampton, W. A., Herdianita, N. R., Holland, G. R., Lynne, B. Y., Martin, R., Newton, Z., Pastars, D., Sannazarro, K. L., and Teece, C. I. A., 2004, Silica phases in sinters and residues from geothermal fields of New Zealand: Earth-Science Reviews, v. 66, no. 1-2, p. 1-61.

Rumble, D., Miller, M. F., Franchi, I. A., and Greenwood, R. C., 2007, Oxygen three-isotope fractionation lines in terrestrial silicate minerals: An inter-laboratory comparison of hydrothermal quartz and eclogitic garnet: Geochimica et Cosmochimica Acta, v. 71, no. 14, p. 3592-3600.

Sánchez-Yañez, C., Reich, M., Leisen, M., Morata, D., Barra, F., 2016, Geochemistry of metalloids in siliceous sinter deposits: Implications for elemental portioning into silica phases: Geochimica et Cosmochimica, *in review*.

Sharp, Z. D., 1990, A laser-based microanalytical method for the in situ determination of oxygen isotope ratios of silicates and oxides. Geochimica et Cosmochimica Acta, v. 54, no. 5, p. 1353-1357.

Sharp, Z. D., Gibbons, J. A., Maltsev, O., Atudorei, V., Pack, A., Sengupta, S., Shock, E. L., and Knauth, L. P., 2016, A calibration of the triple oxygen isotope fractionation in the SiO2–H2O system and applications to natural samples: Geochimica et Cosmochimica Acta, v. 186, p. 105-119.

Sigfusson, B., Gunnarsson, I., Scaling Prevention Experiments in The Hellisheiði Power Plant, Iceland, in Proceedings Thirty-Sixth Workshop on Geothermal Reservoir Engineering, Stanford University, Stanford, California, 2011.

Stapleton, M., Weres, O., Recent Developments in Geothermal Scale Control, in Proceedings Proceedings International Workshop on Mineral Scaling in Geothermal Environments, Manila, Phillippines, 2011, p. 69-76.

Tassi, F., Aguilera, F., Darrah, T., Vaselli, O., Capaccioni, B., Poreda, R. J., and Delgado Huertas, A., 2010, Fluid geochemistry of hydrothermal systems in the Arica-Parinacota, Tarapacá and Antofagasta regions (northern Chile): Journal of Volcanology and Geothermal Research, v. 192, no. 1-2, p. 1-15.

Taylor, H. P., Jr. (1978). Oxygen and hydrogen isotope studies of plutonic granitic rocks. Earth and Planetary Science Letters, 38, 177–210.

Thiemens M. H. and Heidenreich J. E. (1983) The mass independent fractionation of oxygen: A novel isotope effect and its possible cosmochemical implications. Science 219, 1073-1075.

Tobler, D. J., Stefansson, A., and Benning, L. G., 2008, In-situ grown silica sinters in Icelandic geothermal areas: Geobiology, v. 6, no. 5, p. 481-502.

Urey, H., 1947, The Thermodynamic Properties of Isotopic Substances. Liversidge Lecture at The Chemical Society, Royal Institution. December 18, 1946. p. 562-581.

White, D. E; Brannock, W. W., Murata, K. J., 1956, Silica in hot-spring waters: Geochimica et Cosmochimica Acta, v. 10, p. 27-59.

Yanagisawa, N., Matsunaga, I., Sugita, H., Sato, M., and Okabe, T., 2008, Temperature-dependent scale precipitation in the Hijiori Hot Dry Rock system, Japan: Geothermics, v. 37, no. 1, p. 1-18.

Young, E. D., Galy, A. and Nagahara, H., 2002, Kinetic and equilibrium mass-dependent isotope fractionation laws in nature and their geochemical and cosmochemical significance. Geochimica et Cosmochimica Acta, v. 66, no. 6, p. 1095-1104.